This is the peer reviewed author accepted manuscript (post print) version of a published work that appeared in final form in:

Vafaei, Davoud, Ma, Xing, Hassanli, Reza, Duan, Jinming, Zhuge, Yan 2022 'Microstructural and mechanical properties of fiber-reinforced seawater sea-sand concrete under elevated temperatures', Journal of Building Engineering, vol. 50, article no. 104140, pp. 1-22

This output may not exactly replicate the final published authoritative version for which the publisher owns copyright. It is not the copy of record. This output may be used for non-commercial purposes. This version is licensed under a Creative Commons CC-BY-NC-ND 4.0 license (http://creativecommons.org/licenses/by-nc-nd/4.0/).

The final definitive published version (version of record) is available at: 10.1016/j.jobe.2022.104140

Persistent link to the UniSA Research Outputs Repository: 11541.2/27359

General Rights

Copyright and moral rights for the publications made accessible in the UniSA Research Outputs Repository are retained by the authors and/or other copyright owners and it is a condition of accessing publications that users recognize and abide by the legal requirements associated with these rights.

- Users may download and print one copy for the purpose of private study or research.
- You may not further distribute the material or use it for any profit-making activity or commercial gain
- You may freely distribute the persistent link identifying the publication in the UniSA Research Outputs Repository

If you believe that this document breaches copyright, please contact us and provide details. We will remove access to the work immediately and investigate your claim.

Microstructural and mechanical properties of fiber-reinforced seawater sea-sand concrete under elevated temperatures

Davoud Vafaei, Xing Ma*, Reza Hassanli, Jinming Duan and Yan Zhuge
University of South Australia, UniSA STEM, SA 5095, Australia
**Corresponding Author, email address: Xing.Ma@unisa.edu.au*

Abstract
Seawater sea-sand (SWSS) concrete is a promising sustainable construction material that could mitigate the detrimental environmental impact because of the overuse of freshwater and natural sand (FWNS). Physical and chemical properties of seawater sea-sand (SWSS) concrete are significantly different than those of conventional concrete due to a high concentration of certain destructive ions in seawater and sea sand. When a fire accident occurs, the elevated temperature could alter the chemical composition and microstructure of concrete material. This study first examined the effects of elevated temperatures on the pertinent properties of SWSS and FWNS concretes and then proposed methodologies for improving the fire-resistance capability of SWSS concrete by application of fibre additions. Polypropylene (PP) and polyvinyl alcohol (PVA) fibres with volume fractions of 0.1 ~ 0.5% were employed for the above purpose. All the parameters of mass loss, residual thermal strain, compressive strength, elastic modulus, splitting tensile and flexural strength, and fracture toughness of the concrete specimens were examined after exposure to different elevated temperatures ranging from 100 to 750 ℃. Furthermore, the alterations in the microstructure of the mixes after exposure to the elevated temperatures were investigated by X-ray diffraction (XRD) analysis, scanning electron microscopy (SEM) images, water absorption and porosity tests. From the experimental results, the SWSS mix exhibited a lower mass loss, a higher residual thermal strain, and a slightly lower residual compressive strength and elastic modulus and tensile strength than those of conventional FWNS concrete. Additional porosity created by fibre decomposition appears to provide extra rooms for concrete expansion, which led to the formation of finer and lower number of cracks. Generally, incorporation of PP or PVA fibres improved SWSS concrete properties after exposure to the elevated temperatures tested. Compared with PP fibres, PVA fibre was more efficient for improving all the tested concrete properties after the exposure of high temperatures.

Keywords: Seawater, dredged sea-sand, fibre reinforcement, concrete mechanical properties, elevated temperature

1. Introduction

Concrete, as the most widely used construction material mixed from water, gravel, sand and cement, has caused great environmental and health concerns. It was estimated that global carbon dioxide (CO_2) released by construction activities was 7.7 gigatons in 2010, among which 36% was from cement production [1]. Besides CO_2 emission, scarcity of natural resources has been a great concern globally related to concrete production. Both freshwater (FW) and natural sand (NS) are recognised in a process of depletion [2, 3]. Annually about 65.7 km^3 of freshwater is used for concrete production, while it is expected that more than half of the world population will face severe water shortage by 2030 [4]. The

world lands are also disappearing. One of the main reasons behind is the huge mining of sand and gravel for concrete production, where yearly more than 40 billion tons of sand are used in concrete [3]. During the last decades, to minimise the concrete environmental impacts, particularly the greenhouse gases emission, many studies have been carried out to produce cleaner concrete or green concrete [5-7]. One of the successful strategies is to use supplementary cementitious materials (SCMs). The SCMs, such as fly ash (FA), ground granulated blast furnace slag (GGBS), and silica fume (SF), are industrial waste materials with their own environmental challenges. Partial replacement of cement with SCMs helps to reduce CO_2 emission through using less cement, improves concrete performance and mitigating the environmental impacts related to the waste materials [8-10]. To save the valuable FW and NS, research interest in the utilisation of seawater (SW) and sea-sand (SS) for concrete manufacture has been increased recently [11-13].

SW and SS mixed (SWSS) concrete with a partial cement replacement by SCMs is an innovative green concrete with environmental and economic benefits. However, chloride (Cl^-), sodium (Na^+), sulphate (SO_4^{2-}), magnesium (Mg^{2+}), calcium (Ca^{2+}), and potassium (K^+) ions in SW and SS can impose profound impacts on concrete properties as well as reinforcement durability. Based on the 42 publications reviewed recently by Vafaei et al. [14], SW and SS could negatively affect various concrete properties. However, the influence was found generally less than 10%, and could be compensated by the incorporation of fibers [14-16]. Using SW and SS can reduce the workability, setting time, tensile strength, water absorption, sorptivity, porosity and total charge passage (rapid chloride permeability test (RCPT)) of concrete. Furthermore, SWSS concrete has higher early age compressive strength and higher autogenous and drying shrinkage compared with its conventional concrete counterpart. For some of the concrete properties, such as air content and compressive and flexural strengths at an older age, opposite observations were reported. A high concentration of chloride ions in SWSS concrete leads to potential corrosion of reinforcing steel bars. In this case, durable reinforcements such as fibre reinforced polymers (FRPs) were suggested in many studies [17-21].

SWSS concrete can have wide applications in coastal and offshore structures. Due to the harsh environment, the special types of loading, such as wind, waves, currents, tides, earthquakes and ship collisions, and special applications, high-performance concrete is essential for these types of structures. Among all the SWSS concrete properties, fire-resistance capability can be very important, especially for structures related to the oil and gas industry, which are prone to exposure to accidental fires. Fig. 1 shows two examples of fire accidents, which happened in an offshore oil platform in the North Sea and a drilling rig in the Gulf of Mexico. In these two incidents, the explosion and subsequent fires destroyed the structures, leading to the death of 178 people and more than $3 billion property damages [22, 23].



(a) (b)

Fig. 1. (a) The Piper Alpha oil platform and (b) Deepwater Horizon drilling rig accidents [24]

Generally, exposure to fire or any extreme heat source can adversely affect the mechanical properties of any concrete materials. Elevated temperature deteriorates cement past and changes concrete's pore structure. It weakens concrete strengths, causes cracks and spalling, and destroys aggregate-to-cement bond strength [25]. Concrete's mechanical properties rely mainly on the hydration products of calcium hydroxide (portlandite), calcium silicate hydrate (C-S-H) gel. Concrete under fire attack, firstly loses its free or physically bound water, mostly taking place up to 100 ℃. Beyond this temperature, hydration products begin to decompose, and loss of chemically bound water happens. Disintegration of portlandite occurs at around 460 ℃ [26], while C-S-H loses its water over a broad temperature range where the maximum loss takes place at 120 to 160 ℃ [27]. This decomposition process leads to increased total porosity with larger pore sizes within the concrete structure which weakens its strengths and stiffness. Several studies showed that reinforcing concrete by fibres improves its fire-resistance ability [28-35]. At elevated temperatures, fibre melts and makes extra room for concrete expansion. Consequently, the internal vapor pressure partially releases, and the possibility of concrete spalling decreases.

While SWSS concrete is potentially a suitable alternative for conventional concrete for offshore structures, due to the availability of SW and SS in remote areas, the information about SWSS concrete is very limited. Compared with conventional concrete, SWSS concrete has different physical and chemical properties, and its fire-resistance behaviour is not known yet. To the best knowledge of the authors, there is only one published study on the effect of elevated temperatures on the mechanical properties of SWSS concrete. Li et al. [36] reported their findings on the elevated temperature behaviour of alkali-activated slag paste, mortar and concrete using SW and SS. According to this study, the more exposure temperature increased, the more reduction in the residual strengths of paste, mortar and concrete occurred. Residual strength of SWSS slag concrete was slightly lower than fresh water and river sand concrete counterpart. In slag paste, geopolymerization, sintering, and crystallisation resulted in an obvious morphology change. Up to 800 ℃, lower mass loss for SWSS slag concrete were shown compared with freshwater and river sand concrete. Moreover, at high temperatures, the residual thermal strain of the slag concrete was increased by using SW and SS.

From the above literature review, it can be seen that the research on SWSS concrete under elevated temperatures has been rare [36] and there is also no study on the temperature-related properties for the fibre-reinforced SWSS concrete. In this research, various properties of SWSS concrete under elevated temperature have been experimentally tested and compared with FWNS concrete. Effects of the two additives of polypropylene (PP) and polyvinyl alcohol (PVA) fibres at different percentages were examined. The results of the present study would facilitate a reduction of the construction costs of remote offshore structures and at the same time be beneficial for the reduction of CO_2 emission and partially releasing the pressure on the vital natural resources.

2. Test program

2.1. Raw materials

Utilized raw materials were similar to the authors' previous study and have been described extensively in Vafaei et al. [14] and a brief account is provided here. 14 mm crushed basalt was used as coarse aggregates. NS with a maximum nominal size of 2.5-mm and tap water obtained from the Adelaide water supply network were used in the production of conventional concrete. SW and dredged sea-sand (DSS) were collected from coastal areas of South Australia. The concentration of Cl^- and SO_4^{2-} ions in the SW was 19810 and 2824 mg/l, respectively, which is about 360 and 76 times higher than those in the surface waters or drinking water. DSS had a uniform particle size of about 0.25 mm. It contains seashells, grasses and other organic materials, of which only the larger parts were removed by applying a 2 mm sieve before being used in concrete production. Sea-sands can be found in three zones, in beach dry zone, in beach intertidal zone, and sea submersion zone. In this study, the one in the submersion

zone, called DSS, was extracted directly from the seafloor and used in the concrete production. Generally, DSS is dredged and returned to the beach for replenishment purposes. DSS due to its continuous submersion in SW has a pore-water salinity similar to that of SW. However, for the other two zones, the salt content is different. SS in the intertidal zone has higher salt content than DSS, which is due to the evaporation. During low tides, which is the best time for SS collection from the intertidal zone, SW evaporation results in an increase in the near-surface pore-water salinity [37]. Similarly, for the drylands, the wind picks up and transports salt from intertidal zone and sea surfaces and redistributes it across the lands close to the seashore. Therefore, the top layer of the sand in this zone has a considerable concentration of salt.

Ordinary Portland cement (OPC) and GGBS were used as cementitious materials. Both GGBS and cement were mainly composed of SiO_2, Al_2O_3, Fe_2O_3, CaO, and MgO, while the level of SiO_2, Al_2O_3 and MgO is higher in GGBS. Table 1 provides the comparisons for the chemical composition and various properties of these two cementitious materials used in this study. PP and PVA fibres, available in the Australian market were used in the experimental process. Table 2 presents the key properties of the fibres. The specific gravity of the PP is 910 kg/m^3, which is lower than that of 1300 kg/m^3 for PVA. The PP fibres are longer and thicker. The melting point of PP and PVA fibres is 160 and 225 ℃, respectively. Both of the two fibres have excellent chemical, alkali, and corrosion resistance, which made them suitable choices for SWSS concrete.

Table 1. Chemical compositions and physical properties of OPC and GGBS

Cementitious materials	Specific surface area (m^2/kg)	Specific gravity	Chemical Constituent (%)								
			SiO_2	Al_2O_3	Fe_2O_3	CaO	MgO	Na_2O	K_2O	Cl	SO_3
Ordinary Portland Cement	385	3.01	20.5	4.8	3.1	63.5	1.8	0.5	0.54	0.03	2.6
Ground Granulated Blast Furnace Slag	450	2.91	33.01	13.05	0.36	42.70	5.91	-	-	0.00	2.03

Table 2. Physical properties of the PP and PVA fibres

Property	Specific gravity (kg/m^3)	Length (mm)	Diameter (μm)	Thickness (μm)	Tensile strength (MPa)	Young's modulus (GPa)	Chemical resistance	Melting Point	Water Absorption	Alkali Resistance	Corrosion Resistance
PP fibre	910	19	-	56	620-758	3.75	Excellent	160 ℃	Nil	Excellent	Excellent
PVA fibre	1300	8	38	-	1600	40	Excellent	225 ℃	<1% by Weight	Excellent	Excellent

2.2. Mix design and specimens' preparation

The mixes proportions, which were designed recently by the authors of this paper [14], were determined based on trial mixes and considering provisions of Australian design codes for marine structures [38, 39]. For offshore structures, the design compressive strength of concrete should be above 50 MPa [38], the water/binder ratio be less than 0.4 [39] and the cementitious materials content be more than 400 kg/m^3 [39]. Accordingly, a target compressive strength of 55 MPa was considered for the control mix. A water/binder ratio of 0.38 and total cementitious materials of 450 kg/m^3 were used in all mixes. Furthermore, 65% of the cement content were replaced by GGBS. According to the previous literature report, this could significantly reduce the CO_2 emission for the construction of concrete, while GGBS increases concrete's durability without noticeable effects on the strength.

The mixture proportions for all concrete mixes were 158, 292, 1144, 756, and 171 kg/m3 of ordinary Portland cement, GGBS, gravel, NS/SS, and FW/SW, respectively. These mixes are listed in Table 3 based on weight. As shown, a varying amount of MasterGlenium SKY 8700, which is a polycarboxylate ether polymers-based superplasticiser, was used to reach a slump value of 150-200 mm. Compared with PP fibers mixes for a given fiber dosage more superplasticiser was used in mixes with PVA fibers. This is attributed to the hydrophilic nature of the PVA fibers which absorbed a part of the mixing water [40].

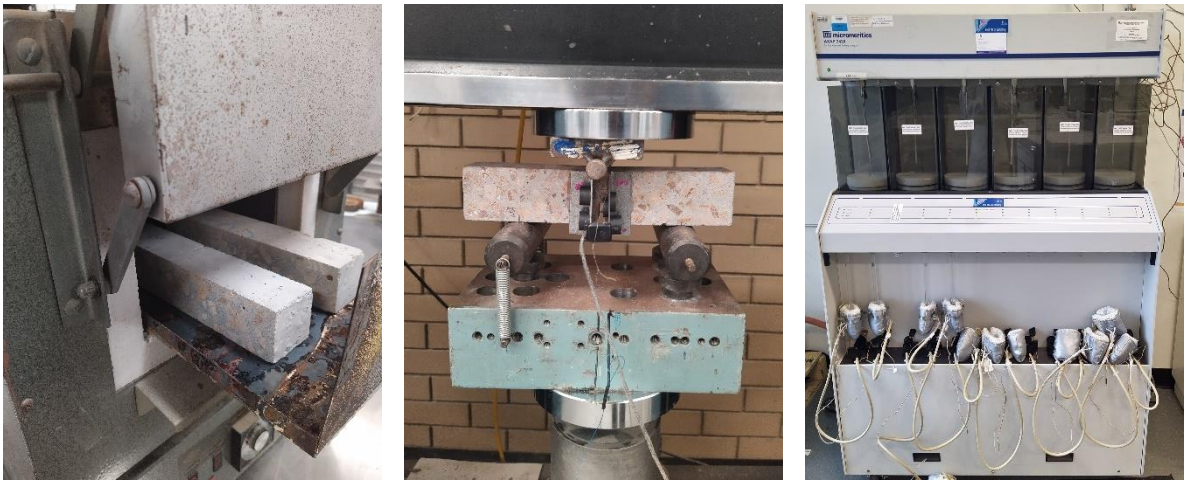
Totally ten mixes, two plain and eight fibre-reinforced concretes were prepared at the concrete laboratory of the University of South Australia. The plain concretes, FWNS was produced using FW and NS, while SWSS was produced using SW and SS. Selection of fiber contents has been a challenging part of the studies related to fiber-reinforced concrete. Using a higher dosage of fiber could significantly increase viscosity of the concrete, resulting in reduction in workability. At the same time, this may affect an even disperse of the fibers [14]. A higher dosage of fiber can also increase the chance of fiber agglomeration, which can negatively influence the mechanical properties of concrete. On the other hand, using a low fiber content might have only a marginal effect on the concrete properties since fibers may not be able to bridge the cracks effectively [40, 41]. Therefore, in this study to reinforce the SWSS mixtures, 0.1, 0.2, 0.3, and 0.5% of PP and PVA fibers (in volume) were added to the SWSS concrete. These relatively lower fibre dosages may guarantee that the samples performance will be less likely affected by improper/insufficient mixing. Note that these percentages were used in the previous studies to investigate the effects of fibres on various SWSS concrete properties [14-16]. The mixes were made according to the Australian code, AS 1012.2 [42]. After casting, the specimens were left in the moulds for 24 hours, then demoulded and moved to a 23 ± 2 ℃ fog room and submerged in lime-saturated water for 28 days.

Table 3. Plain and fibre-reinforced concretes mix design in weight

Concrete mix	Binder		Coarse aggregate	Fine aggregate		Water		superplasticizer	Fibre (%)		Slump (mm)
	Cement	GGBS		NS	SS	FW	SW		PP	PVA	
FWNS	0.35	0.65	2.54	1.68	-	0.38	-	0.020	-	-	195
SWSS	0.35	0.65	2.54	-	1.68	-	0.38	0.020	-	-	190
SWSS-PP0.1	0.35	0.65	2.54	-	1.68	-	0.38	0.020	0.1	-	170
SWSS-PP0.2	0.35	0.65	2.54	-	1.68	-	0.38	0.022	0.2	-	170
SWSS-PP0.3	0.35	0.65	2.54	-	1.68	-	0.38	0.024	0.3	-	180
SWSS-PP0.5	0.35	0.65	2.54	-	1.68	-	0.38	0.029	0.5	-	170
SWSS-PVA0.1	0.35	0.65	2.54	-	1.68	-	0.38	0.023	-	0.1	190
SWSS-PVA0.2	0.35	0.65	2.54	-	1.68	-	0.38	0.027	-	0.2	170
SWSS-PVA0.3	0.35	0.65	2.54	-	1.68	-	0.38	0.030	-	0.3	160
SWSS-PVA0.5	0.35	0.65	2.54	-	1.68	-	0.38	0.039	-	0.5	160

2.3. Test methods

In the present study, after water curing, to reduce early explosive spalling possibility, concrete samples were kept in a 23 ± 2 ℃ room for 15 days and air-dried before exposing to elevated temperatures. Then the specimens were placed in a furnace (Fig. 2(a)) and were heated at a rate of 10 ℃/min from room temperature to four different target temperatures (100, 300, 500, and 750°C). To make sure homogeneous temperature distribution across the samples, the temperature of the furnace was held for an hour after each target temperature. The furnace was then turned off and the specimens were left inside the furnace for 48 hours to cool down naturally to room temperature.



(a) (b) (c)

Fig. 2. a) Furnace, b) fracture toughness test equipment, and c) micromeritics ASAP 2420 System

To determine mass loss and residual thermal strain of the specimens, the mass and length of each specimen were measured before and after exposure to elevated temperatures. For length measurement, four points were specified and numbered at the top and bottom sections of each specimen. The sample's length was measured by using a digital calliper. The compressive strength, elastic modulus, splitting tensile, and flexural strength tests were performed based on the Australian standards, as presented in Table 4. For each type of test, three specimens were tested at each testing temperature.

Table 4. Testing methods used for determining concrete properties

Target properties	Method	Sample shape	Sample dim. (mm)	Number of samples for each temperature
Mass loss	-	Cylinder	100 × 200	3
Residual thermal strain	-	Cylinder	100 × 200	3
Compressive strength	AS 1012.9 [43]	Cylinder	100 × 200	3
Modulus of elasticity	AS 1012.17 [43]	Cylinder	100 × 200	3
Flexural strength	AS 1012.11 [44]	Prism	50 × 50 × 235	3
Splitting tensile strength	AS 1012.10 [45]	Cylinder	100 × 200	3
Fracture toughness	AS 1012.11 [44] & JCI-002-2003 [46]	Prism	50 × 50 × 235	4
Water absorption	AS1012.21 [47]	Disc	100 × 50	3
Porosity	Nitrogen adsorption	Powder	-	-

Three-point bending test on notched beams (50 × 50 × 230 mm with initial notch depth of 25 mm) was performed to examine the fracture toughness behaviour of the concrete mixes after exposure to elevated temperatures (Fig. 2(b)). For each concrete mix at each exposure temperature, four specimens were tested. The tests were carried out on an INSTRON TT-DM–100 kN electronic universal testing machine with the maximum capacity of 100 kN was controlled by a computer. The number of the specimens were selected based on the JCI-002-2003 [46] recommendations. The load was applied at a rate of 0.05 mm/min. An INSTRON 2620-601 dynamic strain gauge extensometer was used for crack mouth opening displacement (CMOD) measurement. During the test, time, load, and CMOD were recorded and the test was terminated at CMOD = 3.5 mm. The fracture energy G_F was calculated from load-CMOD data using the following equations [46]:

$$G_F = \frac{0.75 \times W_0 + W_1}{A_{lig}} \quad (1)$$

$$W_1 = 0.75 \times \frac{S}{L} m \times g \times CMOD_c \quad (2)$$

where W_0 is the energy consumed until the CMOD reaches 3.5 mm (area below CMOD curve), A_{lig} is the area of the ligament and W_1 is the work done by the self-weight of the specimen and experimental equipment such as the steel rod, S is the loading span, L is the length of the specimen, m is the mass of the specimen, g is the gravity acceleration, and $CMOD_c$ is 3.5 mm.

The alterations in the microstructure of concrete specimens after exposure to the elevated temperatures were investigated by X-ray diffraction (XRD), scanning electron microscope (SEM), water absorption and nitrogen adsorption tests. The concrete samples were taken from the inner core of the specimens, then crushed into a fine powder before the XRD test. XRD patterns were recorded by employing a Panalytical Empyrean X-ray diffractometer with a Cu Kα radiation at 40 kV and 40 mA and scan rate of 1.2°/min. The scanning regions were between 2θ values from 5 to 70°. SEM images were obtained from the surface of the inner core samples, performing a Zeiss Crossbeam 540 (Gemini II column). A small piece of concrete was cut and prepared for SEM image. The samples in this study were totally dry through exposure to elevated temperatures. Only room temperature samples were dried for 72 hours in a 30°C oven after being submerged for 24 hours in 75% ethanol. Then all samples were carbon-coated exactly before taking SEM images. The water absorption test was carried out based on the Australian code of AS1012.21 [47]. After the kiln process was completed, the thoroughly cooled concrete discs were weighted before and after 3 days of immersion in water. The results gave an estimation of the total pore volume of the concrete [48, 49]. To gain comprehensive insight on the effects of elevated temperatures on micro-pores, the nitrogen adsorption method was applied to find out the total micro-pores volume of some mixes before and after exposure to 750 ℃. Micromeritics ASAP 2420 surface area and prosing analyser (Fig. 2(c)) was used to determine the total porosity of the concrete mixes from the pores with the width size below 100 nm. For this test, a sample of 50 mg was taken from each concrete mix. Then, the samples were dried at 40 ℃ for 48 hours to remove air and water before testing.

3. Results and discussion

3.1. Mechanical properties

The mechanical properties of the concrete mixes, as tabulated in Table 4, including mass loss, residual thermal strain, compressive strength, elastic modulus, splitting tensile and flexural strength, and fracture toughness were discussed in this section after the concrete mixes being exposed to elevated temperatures.

3.1.1. Mass loss and visual observation

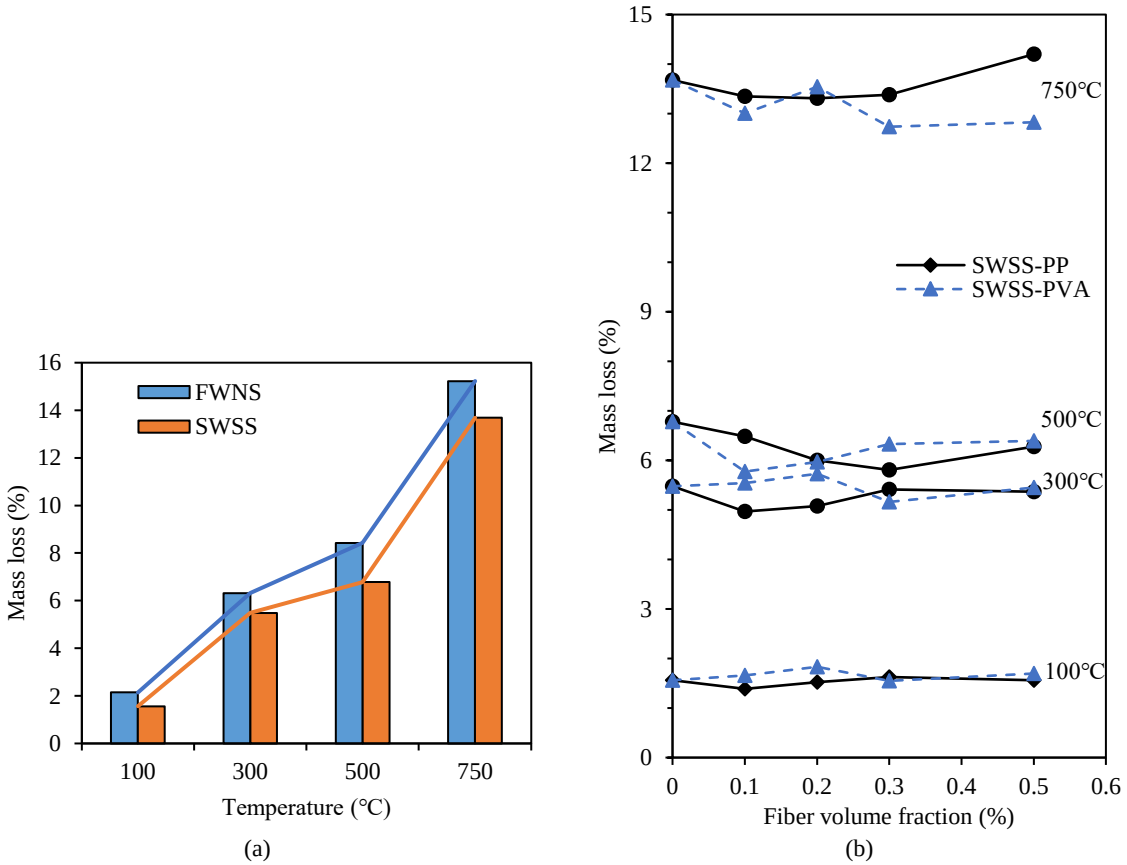
Mass loss of all concrete mixes at 100, 300, 500, and 750°C are presented in Table 5 and Fig. 3. The crack distributions of the plain and fibre-reinforced concrete specimens are displayed in Fig. 4. For fibre-reinforced specimens, the results presented are only for SWSS concrete samples with 0.3% PP/PVA fibre dosage due to space limit. However, the same trend was also observed in other fibre-reinforced samples. For all concrete mixes, more mass loss was observed at higher temperatures. On average, 1.66, 5.45, 6.43, and 13.53% mass reduction were recorded at 100, 300, 500, and 750°C, respectively. In contrast to FWNS, SWSS showed a lower reduction in its mass at all the exposure temperatures as a reflection of the lower content of portlandite and C-S-H than FWNS.

It was reported that for concrete mixes exposed to 100 ℃, the main loss in mass was due to the loss of physically adsorbed water that was weakly bounded [50]. While the mass loss at 300 ℃ is related to the evaporation of the rest of capillary water from macro capillary pores, evaporation of water from gel pores of cement paste, and dehydration of several hydrated products such as C-S-H, ettringite, monosulfoaluminate, and calcium aluminate hydrates [51-54]. The main hydration products of the

concrete containing Ordinary Portland cement and GGBS are C-H, C-S-H, ettringite, aluminate ferrite monosulfate (AFm), a hydrotalcite phase, and occasionally strätlingite (C_2ASH_8) [55]. In SWSS mixes the existing chloride ions could react with AFm to form Friedel's salt ($Ca_4Al_2(OH)_{12}.Cl_2.4H_2O$) [56]. Moreover, the ion exchange between magnesium and calcium led to magnesium hydroxide (brucite) and magnesium silicate hydrate (M-S-H) formation [57]. Friedel's salt can be dehydrated in two separate temperature ranges of 30 - 180 ℃ and 180 - 450 ℃ [58] and M-S-H dehydrates around 120 ℃ similarly as C-S-H [26]. Therefore, part of the mass loss in SWSS mixes at 300 ℃ was due to Friedel's salt and M-S-H disintegration.

Table 5. Mass loss and residual strain of concrete mixes exposed to high temperature

Mix ID	Loss in mass (%)				Residual Thermal Strain ($\times 10^{-3}$)			
	100 ℃	300 ℃	500 ℃	750 ℃	100 ℃	300 ℃	500 ℃	750 ℃
FWNS	2.15%	6.32%	8.43%	15.22%	0.01	0.06	0.55	5.29
SWSS	1.56%	5.48%	6.78%	13.68%	0.05	0.27	2.25	6.77
SWSS-PP0.1	1.39%	4.97%	6.49%	13.35%	0.07	0.33	1.93	6.85
SWSS-PP0.2	1.52%	5.08%	6.00%	13.31%	0.08	0.40	2.16	7.01
SWSS-PP0.3	1.63%	5.42%	5.81%	13.38%	0.12	0.60	2.58	7.23
SWSS-PP0.5	1.56%	5.37%	6.28%	14.20%	0.18	0.91	2.98	7.55
SWSS-PVA0.1	1.66%	5.54%	5.78%	13.01%	0.04	0.22	2.19	6.75
SWSS-PVA0.2	1.83%	5.73%	5.97%	13.55%	0.05	0.23	2.01	6.56
SWSS-PVA0.3	1.55%	5.16%	6.33%	12.74%	0.02	0.10	1.86	5.99
SWSS-PVA0.5	1.74%	5.46%	6.40%	12.83%	0.01	0.03	1.74	5.47



(a) (b)

Fig. 3. Percentage of mass loss for a) plain and b) fibre-reinforced mixes

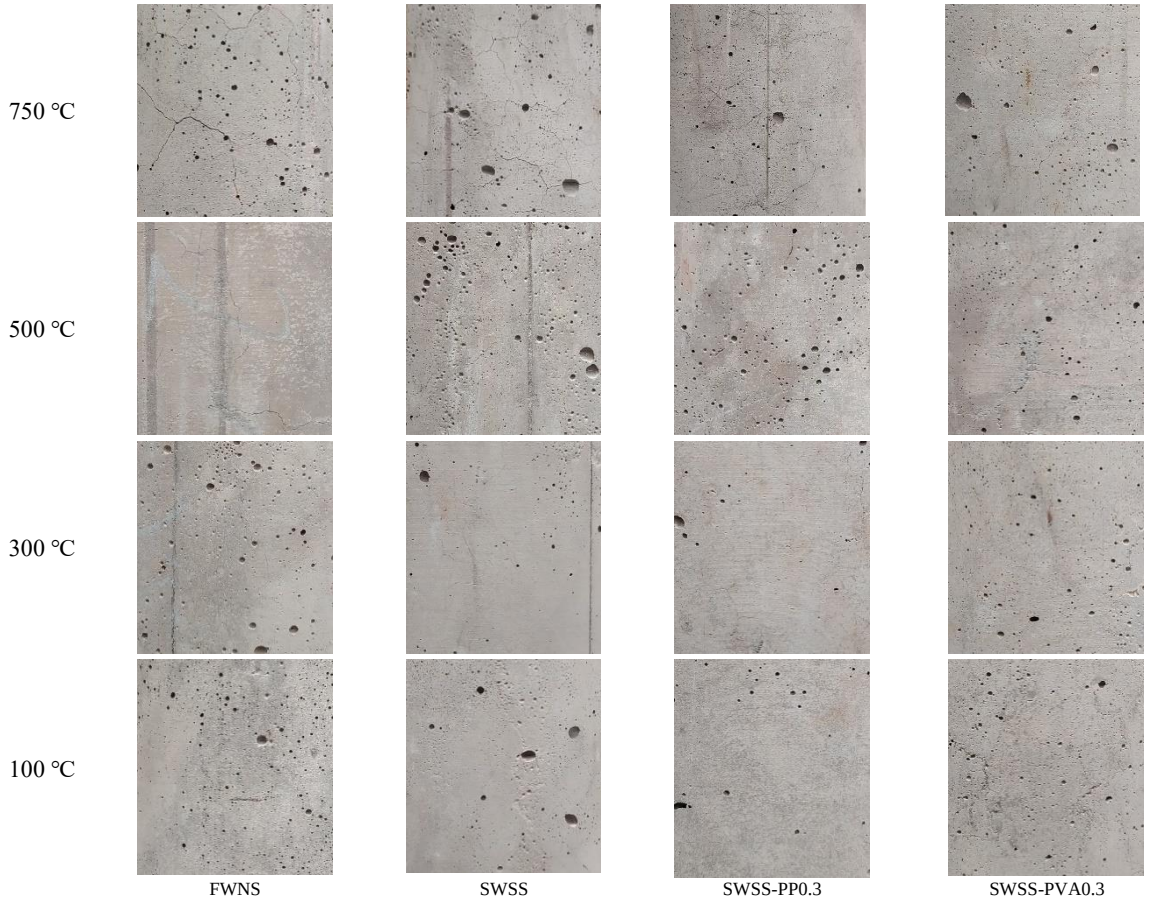


Fig. 4. Optical images of concrete surfaces after exposure to high temperatures

Portlandite and brucite started to dehydrate at about 460 and 420 ℃ [26], respectively. Therefore, at 500 ℃, besides continuous decomposition of C-S-H, M-S-H and Friedel's salt, dehydration of portlandite and brucite led to further loss in specimens' mass. The above dehydration processes also resulted in the formation of fine cracks in plain concrete mixes (FWNS and SWSS) (see Fig. 4). Magnesite ($MgCO_3$) decomposed to MgO and CO_2 between 500 to 600 ℃ and $CaCO_3$ (calcite and aragonite) decomposed between 600 to 800 ℃ [26]. At 750 ℃, in addition to continuous dehydration of hydrates (portlandite, brucite, C-S-H, M-S-H and Friedel's salt) decarbonisation of $CaCO_3$ [59] and magnesite [56] made a significant reduction in concrete weight and consequently more cracks were formed (Fig. 4).

During fibre-reinforced concretes kilning, dense and black smoke was emitted from the chimney of the furnace at a temperature between 200 to 350 ℃, probably from the decomposition of PP and PVA fibres. As shown in Fig. 3(b), the effects of fibres on mass loss at 100 ℃ were marginal, and on average, only 1.6% reduction in mass was observed. At a higher temperature, mixes with both types of fibres showed less mass loss compared to SWSS with an exception for SWSS-PVA0.1, SWSS-PVA0.2 and SWSS-PP0.5. SWSS-PVA0.1 and SWSS-PVA0.2 at 300 ℃ and SWSS-PP0.5 at 750 ℃ showed only slightly higher losses. Moreover, less cracks with finer width were formed for fibre-reinforced SWSS mixes at elevated temperatures as shown in Fig. 4. These observations could be attributed to the small narrow channels created by the decomposition of PP and PVA fibres which might partially release the internal vapour pressure from the concrete. Moreover, a lower number of cracks were observed in specimens with PVA fibres than SWSS-PP mixes. The reasons might be the shorter length and lower thickness/diameter of the PVA fibres compared with PP, which led to a larger number of PVA fibres than PP at the same fibre volume fraction. The larger number of PVA could form more uniform expansion channels throughout the concrete mass after PVA fibre melting. Besides, another potential

reason that could be the case in samples with higher fibre dosages is non-uniform dispersion of PP fibre caused by improper mixing. However, as mentioned earlier due to a relatively lower fibre dosages used in this study (<< 0.5%) it could not be the reason. There was most likely a proper mixing and sufficient fibre distribution for both types of fibre. According to the results, no noticeable relationship between fibre content increasing and mass loss percentage was observed.

3.1.2. Residual thermal strain

The residual strain of the plain and fibre-reinforced concrete mixes, after exposure to elevated temperatures, are presented in Table 5 and Fig. 5. In general, the higher residual strain was obtained at a higher temperature. The average residual strain of all mixes after being exposed to a temperature of 100, 300, 500, and 750°C were 0.06, 0.31, 2.03, and 6.54 ($\times 10^{-3}$) expansion, respectively. As shown in Fig. 5(a), despite the exposure temperature, higher residual strains were shown for SWSS compared with those of FWNS. The residual strain of the SWSS mix increased by adding PP fibre and decreased by adding PVA fibre. Moreover, when the content of the added fibres increased, a higher increase in residual strain was observed for SWSS-PVA and a higher decrease in residual strain was observed for SWSS-PP.

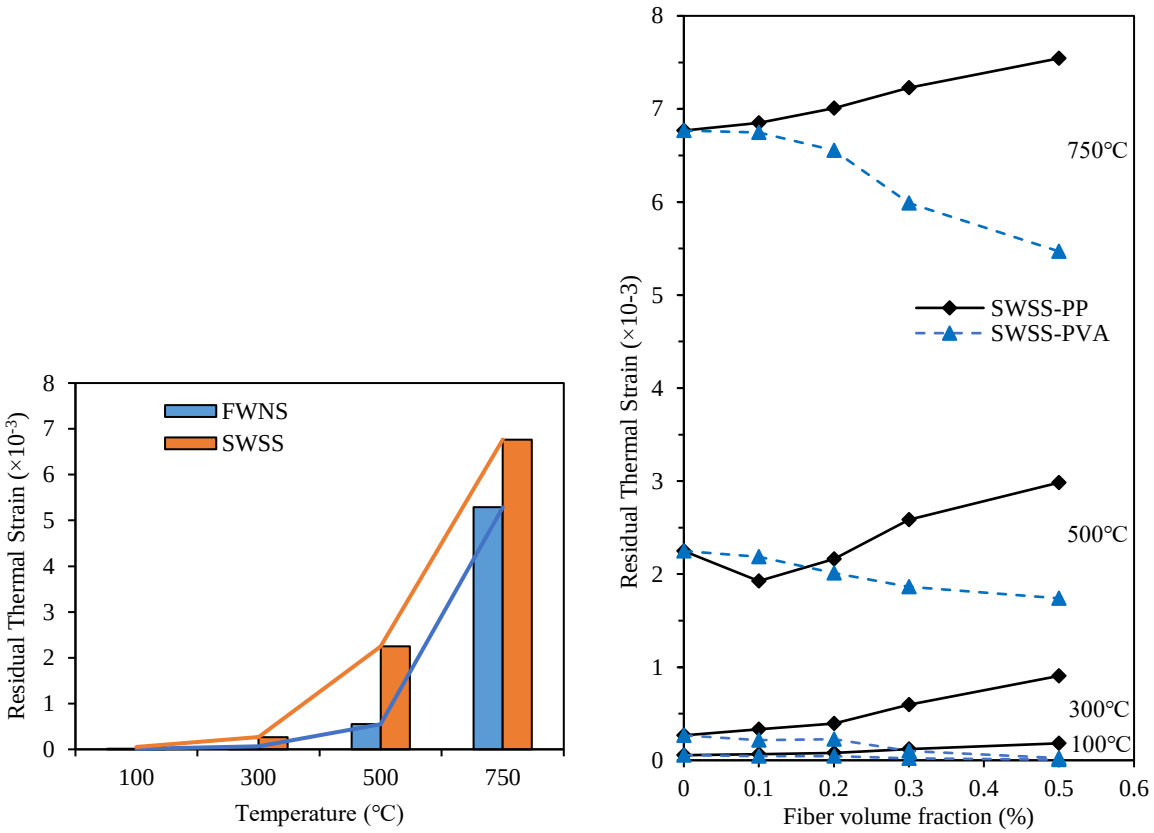


Fig. 5. Residual thermal strain for a) plain and b) fibre-reinforced mixes

3.1.3. Compressive strength

Compressive strength results of all specimens exposed to elevated temperatures are presented in Table 6 and Fig. 6. As shown, increasing the temperature from 23 to 750 °C led to a progressive reduction in compressive strength, which is in line with the findings of the other studies about the effect of elevated

temperatures on the different types of concrete [60, 61]. The average residual strength of concrete mixes at 100, 300, 500, and 750°C were 87%, 80%, 66% and 26% of the SWSS strength at room temperature, respectively.

At all elevated temperatures tested, slightly lower residual strength was exhibited by SWSS compared with FWNS, which could be attributed to the lower C-S-H content of SWSS compared to FWNS [56]. Adding PP fibre to the SWSS mix resulted in a decrease in the compressive strength at all the temperatures. In addition, a higher reduction strength occurred with increasing PP fibre content. These observations are in line with the findings from the previous studies [62, 63] and could be related to the additional porosity caused by fibre melting. For specimens with PVA fibre, despite the porosity increment, an increase in the compressive strength was observed. This could be attributed to (i) the chemical bonding of the PVA with cement hydration products compared with the physical bonding of PP, (ii) more uniform distribution of the PVA through the concrete and (ii) superior mechanical properties of PVA such as higher tensile strength, higher elastic modulus, and higher melting point compared with PP.

Table 6. Compressive strength test results

Mix ID	Compressive strength (MPa)								
	23 ℃	100 ℃		300 ℃		500 ℃		750 ℃	
FWNS	54.3	47.3	(-5.31%)	40.2	(-19.55%)	39.0	(-21.94%)	15.3	(-69.38%)
SWSS	50.0	43.3	(-13.38%)	39.4	(-21.11%)	35.6	(-28.81%)	11.9	(-76.16%)
SWSS-PP0.1	50.2	42.9	(-14.11%)	39.4	(-21.17%)	33.1	(-33.87%)	12.4	(-75.25%)
SWSS-PP0.2	48.9	40.2	(-19.62%)	38.3	(-23.32%)	28.7	(-42.69%)	12.5	(-75.02%)
SWSS-PP0.3	48.1	40.1	(-19.72%)	37.6	(-24.87%)	27.3	(-45.49%)	11.9	(-76.25%)
SWSS-PP0.5	44.1	37.8	(-24.5%)	36.4	(-27.19%)	26.7	(-46.52%)	12.7	(-74.6%)
SWSS-PVA0.1	50.5	43.6	(-12.87%)	39.9	(-20.29%)	34.6	(-30.72%)	12.4	(-75.18%)
SWSS-PVA0.2	51.3	45.4	(-9.28%)	41.0	(-17.98%)	33.6	(-32.84%)	13.0	(-74.08%)
SWSS-PVA0.3	52.0	46.4	(-7.2%)	43.9	(-12.17%)	34.9	(-30.16%)	13.8	(-72.49%)
SWSS-PVA0.5	53.4	47.3	(-5.47%)	44.5	(-11.05%)	35.9	(-28.29%)	14.1	(-71.76%)

Note: The number in the () shows the percentage of strength decrease or increase over that of the SWSS mix at 23 ℃.

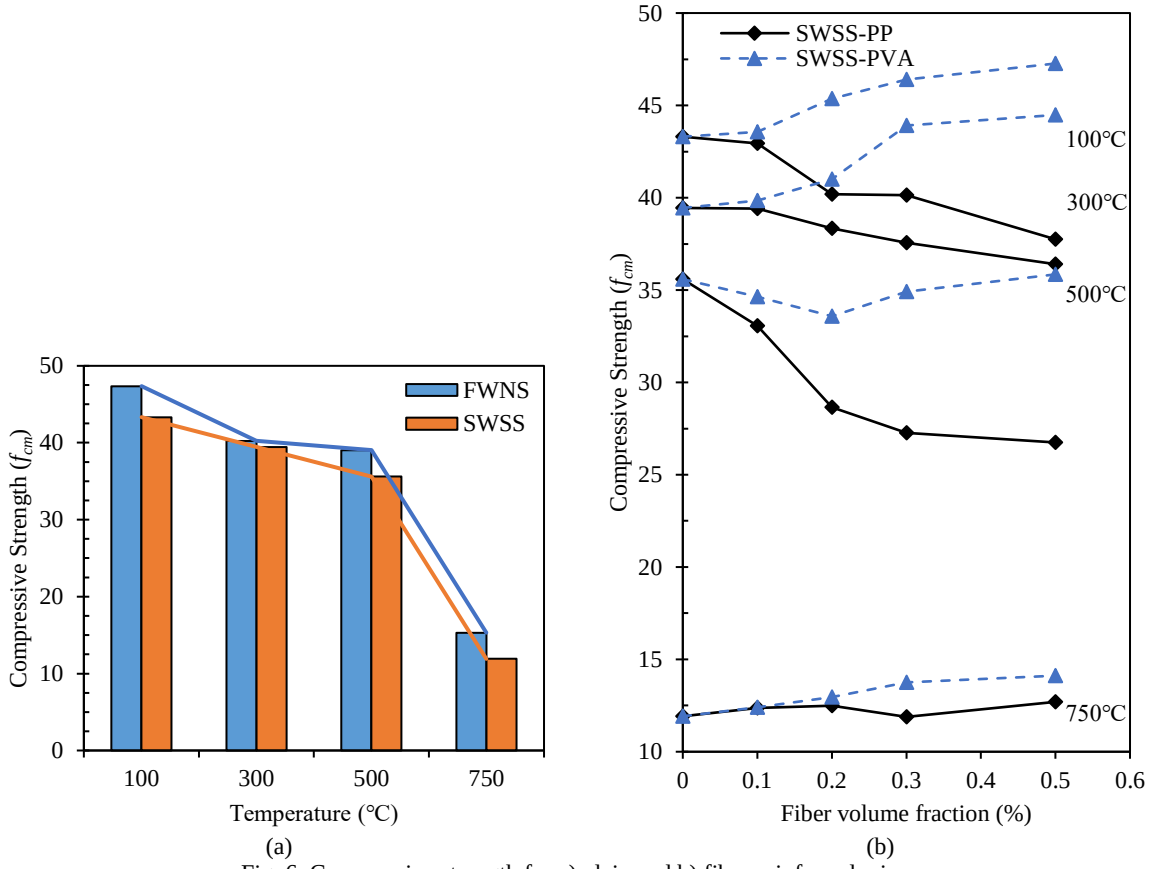


Fig. 6. Compressive strength for a) plain and b) fibre-reinforced mixes

The failure mode of the plain and fibre-reinforced concrete specimens exposed to elevated temperatures under uniaxial compression tests are presented in Fig. 7. For fiber-reinforced specimens, the results presented are only for SWSS concrete samples with 0.3% PP/PVA fiber dosage due to space limit. However, the same trend was also observed in other fibre-reinforced samples. For all concrete mixes, a combination of splitting and shear failures occurred. Fibre-reinforced mixes, regardless of the exposure temperature, preserved their integrity.



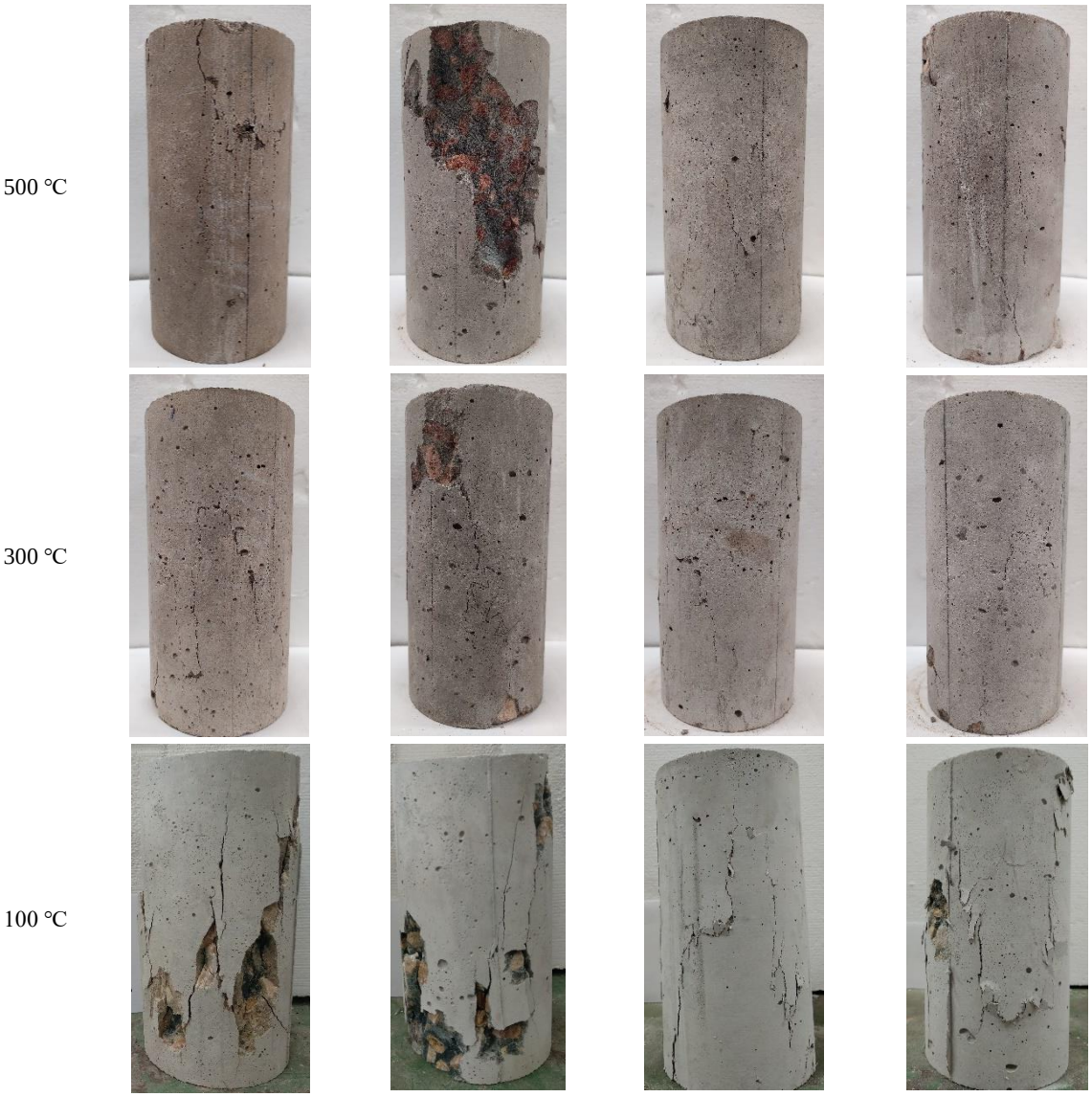


Fig. 7. Failure mode of concrete specimens under compressive strength test after exposure to high temperatures

3.1.4. Elastic modulus

Effects of elevated temperature on the elastic modulus of concrete specimens are presented in Table 7 and Fig. 8. This property was determined prior to concrete cracking and in the stress level of 40% of the compressive strength. As shown, for all mixes, the elastic modulus decreased as the temperature increased. After an exposure to 100, 300, 500, and 750°C, the elastic modulus of the mixes in average was reduced to 88%, 65%, 32% and 20% that of SWSS at room temperature. This observation is in line with the findings from [64-66]. At all the exposure temperatures, the SWSS mix showed lower elastic modulus than FWNS. The difference increased at a higher temperature potentially because of the different composition of sea-sand from normal sand. Furthermore, the effect of fibre addition on the elastic modulus was marginal, regardless of the fibre type and content. For example, the modulus of elasticity of the fibre-reinforced SWSS mixes at 500 ℃ varied from 27% to 33% of that of the SWSS at room temperature.

Table 7. Elastic modulus test results

Mix ID	Elastic modulus (GPa)								
	23 ℃	100 ℃		300 ℃		500 ℃		750 ℃	
FWNS	37.76	34.06	(-6.86%)	26.36	(-27.91%)	16.13	(-55.9%)	7.46	(-79.59%)
SWSS	36.57	33.13	(-9.41%)	23.13	(-36.74%)	12.32	(-66.31%)	6.11	(-83.3%)
SWSS-PP0.1	36.23	32.65	(-10.72%)	23.44	(-35.9%)	11.33	(-69.01%)	6.67	(-81.77%)

SWSS-PP0.2	35.32	31.58	(-13.65%)	24.14	(-34%)	11.74	(-67.9%)	7.04	(-80.74%)
SWSS-PP0.3	35.20	31.35	(-14.27%)	24.59	(-32.76%)	12.00	(-67.19%)	7.46	(-79.59%)
SWSS-PP0.5	34.84	31.12	(-14.9%)	24.40	(-33.28%)	12.14	(-66.8%)	7.72	(-78.9%)
SWSS-PVA0.1	35.96	32.13	(-12.14%)	21.83	(-40.3%)	11.00	(-69.92%)	7.54	(-79.38%)
SWSS-PVA0.2	36.13	32.23	(-11.87%)	23.64	(-35.37%)	10.71	(-70.7%)	7.14	(-80.47%)
SWSS-PVA0.3	35.23	31.70	(-13.32%)	24.11	(-34.08%)	10.00	(-72.66%)	8.20	(-77.59%)
SWSS-PVA0.5	34.24	30.81	(-15.75%)	23.38	(-36.06%)	10.63	(-70.95%)	8.47	(-76.83%)

Note: The number in the () shows the percentage of elastic modulus decrease or increase over that of the SWSS mix at 23 °C.

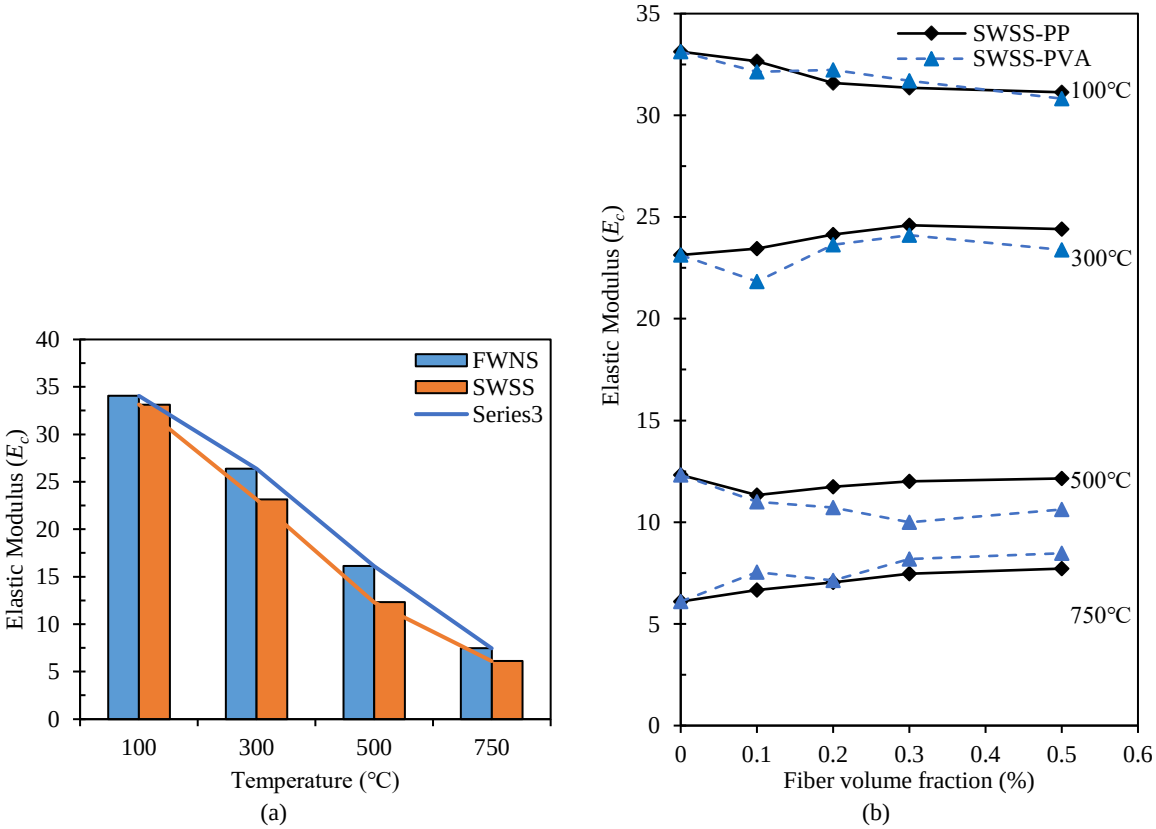


Fig. 8. Elastic modulus for a) plain and b) fibre-reinforced mixes

3.1.5. Flexural and splitting tensile strength

Flexural and split tensile strengths of the specimens after exposure to the elevated temperatures are presented in Tables 8 and 9, and Figs. 9 and 10. For both flexural and split tensile strengths, similar to compressive strength, increase in the exposure temperature led to a decrease in these strengths. At 100, 300, 500, and 750°C the average flexural strength of the mixes was 95%, 71%, 41%, and 11% of that of SWSS at 23 °C, respectively. At all the exposure temperatures, almost similar flexural strengths were observed for both SWSS and FWNS plain concretes. However, the tensile strengths of SWSS were lower than FWNS.

Adding fibre led to an increase in both flexural and tensile strengths at all the exposed temperatures. Both PP and PVA fibres had higher durability at 100 °C [67, 68]. Therefore, at 23, 100 and before 300 °C, fibre existence increased flexural and tensile strengths of the fibre-reinforced mixes. Fibres crossed over the two sides of the cracks and made a lateral constraint and confinement. At 100 °C, for the mixes with both types of fibres strength increases were observed as the fibre content increased. The addition of 0.3% of PP/PVA showed the highest strength at 100 °C among all fibre dosages. As shown in Figs. 9(b) and 10(b), from 300 to 750 °C, similar trends in flexural and tensile strength variation of the specimens exhibited. An increase in strengths was observed with 0.1% fibre addition, then strengths decreased as the fibre content increased. This observation could be attributed to the additional porosity

in fibre-reinforced mixes, where fibres decomposition made enough room for concrete to expand at elevated temperatures, released the internal pressure and limited crack formation. By increasing fibre content, the negative effects of this additional porosity became more dominant and a decreasing trend in flexural and tensile strengths were observed after the initial increment from 0.1% fibre incorporation. Compared with PP fibre, better performance in flexural and tensile strength improvement was shown at all the temperatures by PVA fibres. The reason could be (i) higher tensile strength and modulus of elasticity of PVA, (ii) PVA's strong chemical bonding with cement products compared to the physical bond of PP, and (iii) a relatively larger number and more uniform distribution of PVA fibres within the solid concrete.

Table 8. Flexural strength test results

Mix ID	Flexural strength (MPa)								
	23 ℃	100 ℃		300 ℃		500 ℃		750 ℃	
FWNS	6.60	5.86	(-12.39%)	4.60	(-31.24%)	2.22	(-66.87%)	0.74	(-88.99%)
SWSS	6.69	5.78	(-13.65%)	4.44	(-33.58%)	2.35	(-64.92%)	0.60	(-91.1%)
SWSS-PP0.1	6.69	6.04	(-9.72%)	4.80	(-28.22%)	2.93	(-56.19%)	0.78	(-88.34%)
SWSS-PP0.2	7.06	6.41	(-4.23%)	4.84	(-27.63%)	2.75	(-58.88%)	0.71	(-89.38%)
SWSS-PP0.3	7.27	6.62	(-1.08%)	4.62	(-30.92%)	2.42	(-63.81%)	0.60	(-91.03%)
SWSS-PP0.5	7.15	6.46	(-3.44%)	4.39	(-34.35%)	2.35	(-64.85%)	0.55	(-91.77%)
SWSS-PVA0.1	6.82	6.32	(-5.48%)	5.20	(-22.24%)	3.36	(-49.76%)	0.92	(-86.24%)
SWSS-PVA0.2	7.24	6.46	(-3.43%)	5.12	(-23.44%)	3.22	(-51.85%)	0.82	(-87.74%)
SWSS-PVA0.3	7.51	6.77	(1.27%)	5.00	(-25.23%)	3.11	(-53.5%)	0.76	(-88.64%)
SWSS-PVA0.5	6.92	6.56	(-1.87%)	4.81	(-28.1%)	2.66	(-60.26%)	0.72	(-89.28%)

Note: The number in the () shows the percentage of strength decrease or increase over that of the SWSS mix at 23 ℃.

Table 9. Splitting tensile strength test results

Mix ID	Splitting tensile strength (MPa)								
	23 ℃	100 ℃		300 ℃		500 ℃		750 ℃	
FWNS	4.82	4.46	(1.28%)	3.94	(-10.53%)	2.95	(-33.01%)	1.33	(-69.8%)
SWSS	4.40	3.90	(-11.44%)	3.26	(-25.97%)	2.10	(-52.31%)	0.86	(-80.47%)
SWSS-PP0.1	4.60	4.10	(-6.9%)	3.39	(-22.95%)	2.56	(-41.89%)	0.91	(-79.33%)
SWSS-PP0.2	4.76	4.40	(-0.08%)	3.36	(-23.7%)	2.48	(-43.68%)	0.93	(-78.88%)
SWSS-PP0.3	5.15	4.54	(3.1%)	3.27	(-25.74%)	2.29	(-48%)	0.97	(-78.04%)
SWSS-PP0.5	4.91	4.60	(4.46%)	2.91	(-33.83%)	1.98	(-54.96%)	1.00	(-77.35%)
SWSS-PVA0.1	4.66	4.20	(-4.63%)	3.68	(-16.51%)	2.64	(-40.09%)	1.03	(-76.52%)
SWSS-PVA0.2	5.13	4.70	(6.73%)	3.59	(-18.48%)	2.56	(-41.87%)	0.99	(-77.52%)
SWSS-PVA0.3	5.42	5.00	(13.54%)	3.55	(-19.39%)	2.51	(-43%)	0.95	(-78.54%)
SWSS-PVA0.5	5.11	4.70	(6.73%)	3.47	(-21.15%)	2.22	(-49.53%)	0.82	(-81.27%)

Note: The number in the () shows the percentage of strength decrease or increase over that of the SWSS mix at 23 ℃.

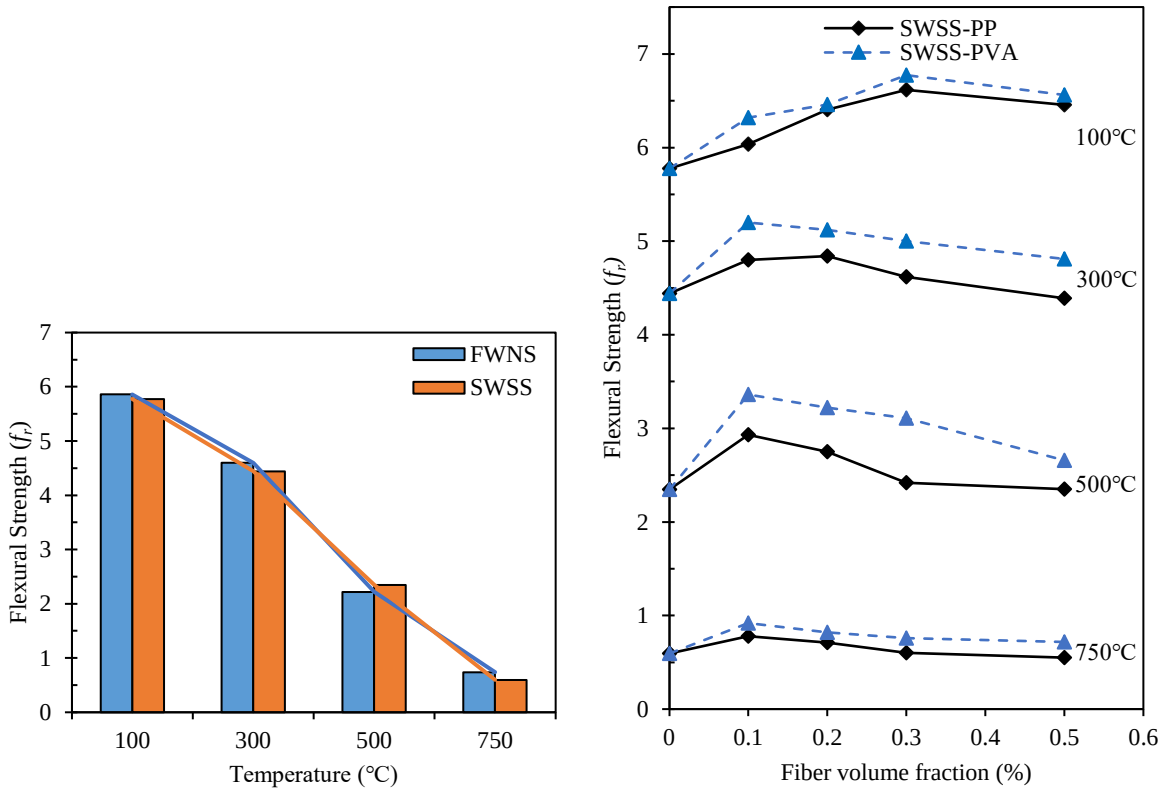


Fig. 9. Flexural strength for a) plain and b) fibre-reinforced mixes

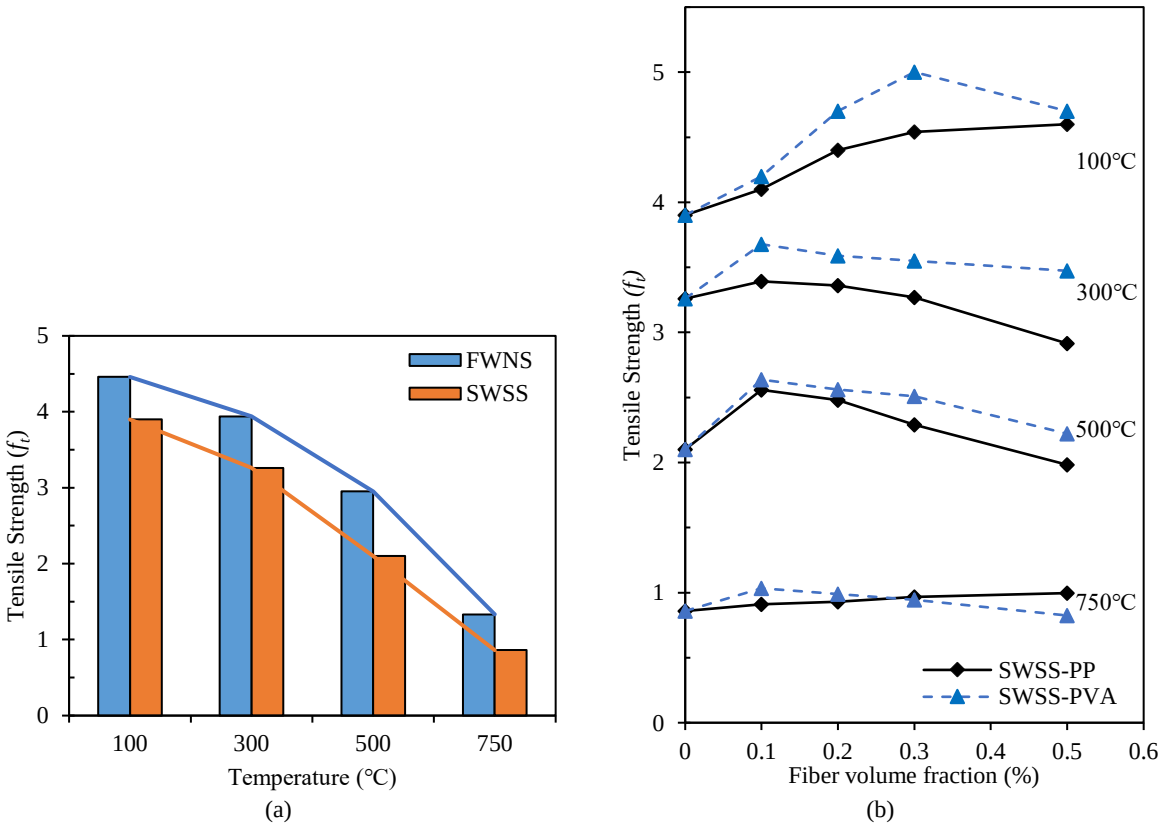


Fig. 10. Tensile strength for a) plain and b) fibre-reinforced mixes

3.1.6. Fracture toughness

The load-CMOD curves obtained from the flexural tests of FWNS, SWSS, SWSS-PP0.5, and SWSS-PVA0.5 mixes after exposure to elevated temperatures are presented in Fig. 11. For two plain concretes at all the exposure temperatures very similar behaviours were observed. At low temperatures, similar peak loads, poor post-cracking performance with a brittle failure mode exhibited. For all the mixes, as the exposure temperature increased the peak flexural load decreased. Interestingly, by increasing the exposure temperature, similar to the modulus of elasticity, the linear parts slop (pre-crack) decreased and the CMOD corresponding to peak loads was shifted to the right side, i.e., with higher values. The maximum flexural load for FWNS mix at 23 ℃, 100, 300, 500, and 750°C occurred at varying CMODs of 0.060, 0.151, 0.136, 0.292, and 0.498 mm, respectively; for SWSS the corresponding CMODs were 0.065, 0.151, 0.176, 0.495, and 0.643 mm, respectively. Furthermore, as the temperature increased a wider load-CMOD curve with a more ductile behaviour was achieved, rather than a sharp drop with a brittle failure at room temperature. For example, the residual strength of the FWNS and SWSS at 100 ℃ were 0.067 and 0.066 kN at the CMOD of 1.5 mm, respectively, while at the same CMOD level, the residual strength at 500 ℃ increased to 0.108 and 0.162 kN, respectively.

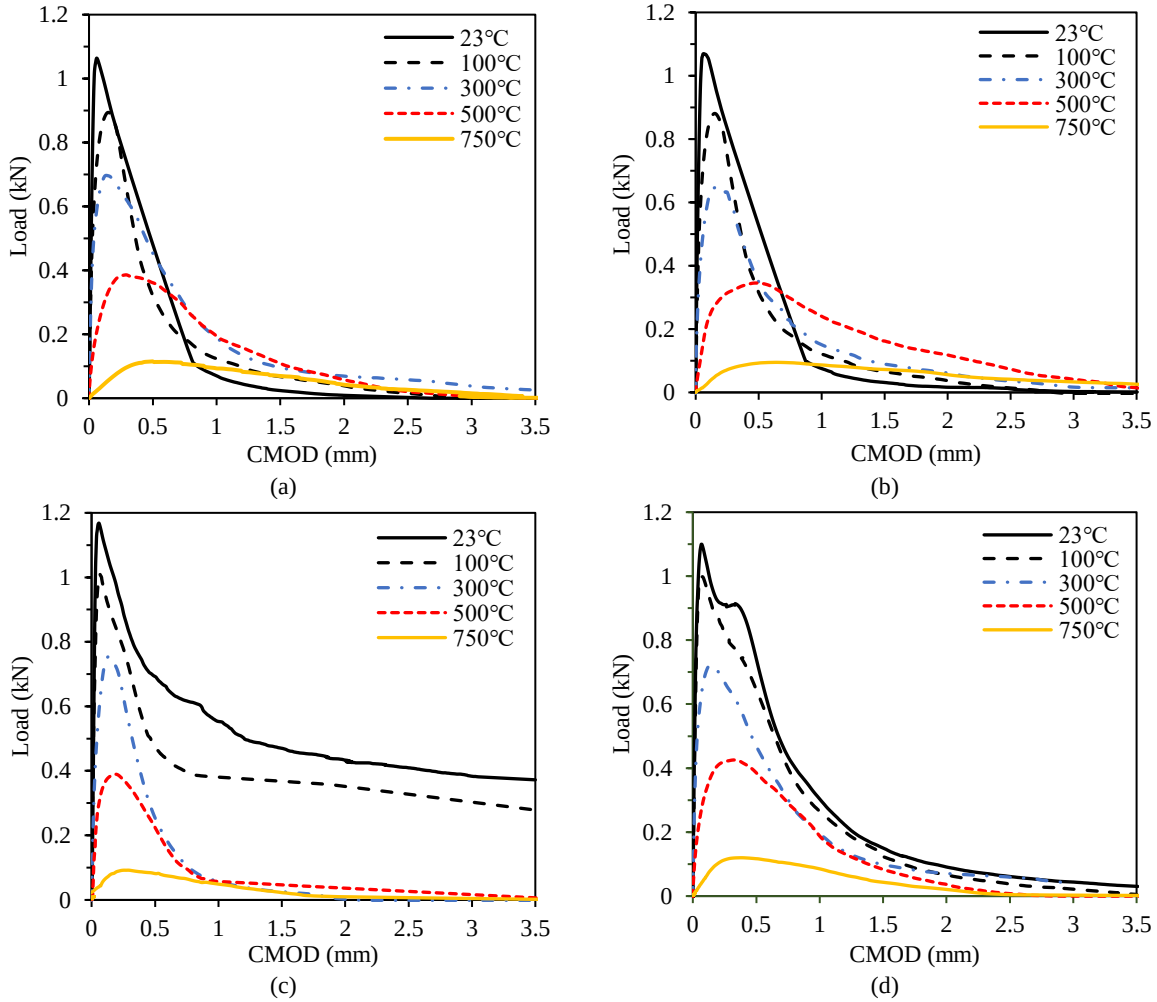


Fig. 11. Load-CMOD curve of a) FWNS, b) SWSS, c) SWSS-PP0.5, and d) SWSS-PVA0.5 mixes exposed to high temperatures

Similar to plain concretes, for all SWSS mixes with fibres the peak flexural loads decreased and the corresponding CMODs were shifted to higher values as the exposure temperature increased. For

example, the peak loads for SWSS-PP0.5 at 23 ℃, 100, 300, 500, and 750°C were 1.168, 1.009, 0.755, 0.389, and 0.092 kN, respectively, where the corresponding CMODs were 0.057, 0.064, 0.134, 0.184, and 0.285 mm, respectively. At room temperature and 100 ℃, PP fibre addition led to an increased ductility and post-crack residual strength. PVA fibres had minor effects on the toughness behaviour. When CMOD equalled 1.5 mm, the residual loads for SWSS-PP0.5 mix at 23 and 100 ℃ were 0.470 and 0.368 kN, respectively, while for SWSS-PVA0.5 the residual loads were as low as 0.150 and 0.137 kN, respectively. At higher temperatures, fibre melting, and the additional porosity caused by fibre decomposition led to a decrease in ductility and post-crack residual load of the SWSS-PP mix. Unlike PP, the PVA mixed concrete exhibited similar behaviour to that of plain SWSS mix.

Fracture energy of the concrete mixes after exposure to elevated temperatures are presented in Fig. 12. As shown in the figure, for all the exposure temperatures, the fracture energy of the FWNS and SWSS was almost similar. Interestingly, although the peak flexural load decreased as the temperature increased from 23 to 500 ℃, almost similar fracture energy was obtained. This is likely because of the increased ductility that compensated load reduction effects. The fracture energy of FWNS after exposure to 23 ℃, 100, 300, 500, and 750°C were 0.28, 0.27, 0.34, 0.24, and 0.11 N/mm, respectively; those of SWSS were 0.31, 0.27, 0.29, 0.30, and 0.12 N/mm, respectively. The incorporation of fibres resulted in a significant improvement in the fracture energy of the SWSS mixes at 23 and 100 ℃. The fracture energy of SWSS mix with 0.5% PP fibre was 214% and 183% higher than those of SWSS mix at 23 and 100 ℃, respectively. While those of SWSS-PVA0.5 were 62% and 61% higher than SWSS, respectively. At higher temperatures, a lower or the same fracture energy was obtained for mixes with PP and PVA fibres.

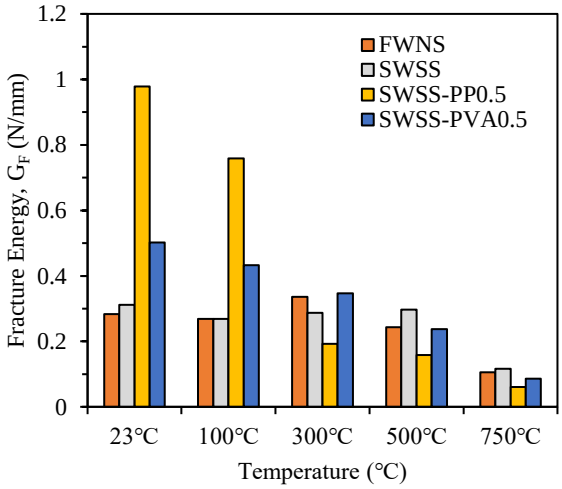


Fig. 12. Fracture energy of SWSS, FWNS, SWSS-PP0.5, and SWSS-PVA0.5 mixes

3.2. Microstructure

3.2.1. XRD analysis

Figs. 13(a) and 13(b) shows the XRD results of FWNS and SWSS concrete mixes at room temperature and after exposure to 500 ℃. Quartz sand (SiO_2) was a major component and was identified by the characteristic peaks in the XRD pattern. Together with quartz, portlandite, C-S-H, calcite, unhydrated calcium silicates (C_2S and C_3S), tricalcium aluminate (C_3A), and ettringite were identified from FWNS and SWSS, which are the expected products formed by cement hydration. In a concrete with cement blended with GGBS, a hydrotalcite phase, and occasionally strätlingite (C_2ASH_8) could be formed [55], likely due to their low amount in the concrete mix, it is not easy to detect from the XRD patterns. As mentioned earlier, existing chloride ions in SWSS reacted with aluminate ferrite monosulfate (AFm)

hydrate to form Friedel's salt [56]. As shown in Figs. 13(a) and 13(b), Friedel's salt is the main difference between FWNS and SWSS that can be detected from these XRD patterns. Because brucite, M-S-H, and magnesite in SWSS concrete are to be detected in angles that are coupled with the other existing peaks, they are hard to be identified through these XRD patterns.

After exposure to 500 ℃ a reduction in portlandite, C-S-H, and ettringite peaks was observed. This was due to the decomposition of the cement hydration products. This decomposition led to a mass loss coupled with an increase in porosity as well as strength reduction of the concrete mixtures after exposure to elevated temperatures. In addition, it is worth noting that Friedel's salt peak completely disappeared at 500 ℃ from the XRD pattern of the SWSS mix. This observation indicates that dehydration happened prior to this temperature, which appears to be in line with the findings of [58]. As shown in Figs. 13(a) and 13(b), C-S-H peaks height in SWSS are lower than those of FWNS. This reflects the lower content of these hydration products in SWSS compared with FWNS and explains the lower loss in mass and lower strength in SWSS.

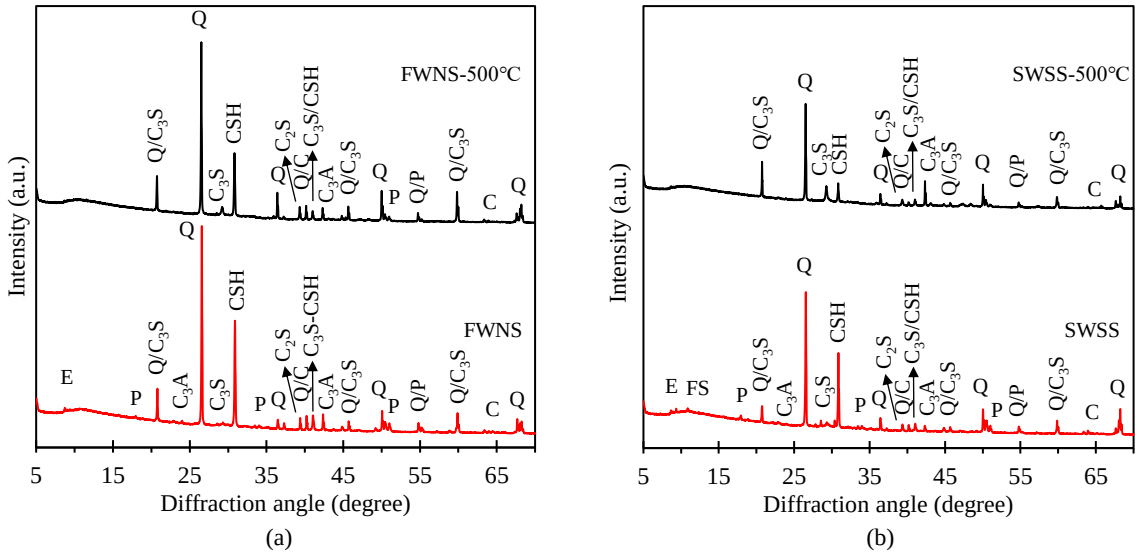


Fig. 13. X-ray diffraction (XRD) patterns of (a) FWNS and (b) SWSS mixes after exposure to 23℃ and 500℃ (E: ettringite, P: portlandite, Q: quartz, C: calcite, B: brucite, FS: Friedel's salt)

3.2.2. Microstructures (SEM)

Fig. 14 shows the SEM image of the FWNS and SWSS mixes in a room environment before and after exposure to 500 ℃. For both mixes at 23 ℃, Portlandite and C-S-H are the main hydration products. In the SWSS mix, plate-like crystals of Friedel's salt, as well as needle-like crystals of ettringite, could be observed. After exposure to 500 ℃, the surface became looser and certain micropores appeared. The decomposition of portlandite and C-S-H led to a weaker and porous structure. Furthermore, aragonite and calcite crystals were observed on the 500 ℃ samples, which must have been decarbonated at higher temperatures. In the case of fibres, as mentioned earlier, it can be expected that at 500 ℃ both types of fibres decomposed. Fig. 15 shows the fibre beds in SWSS-PP and SWSS-PVA mixes. As expected, no fibre existed at this temperature and many micro- and nano-cracks were developed.

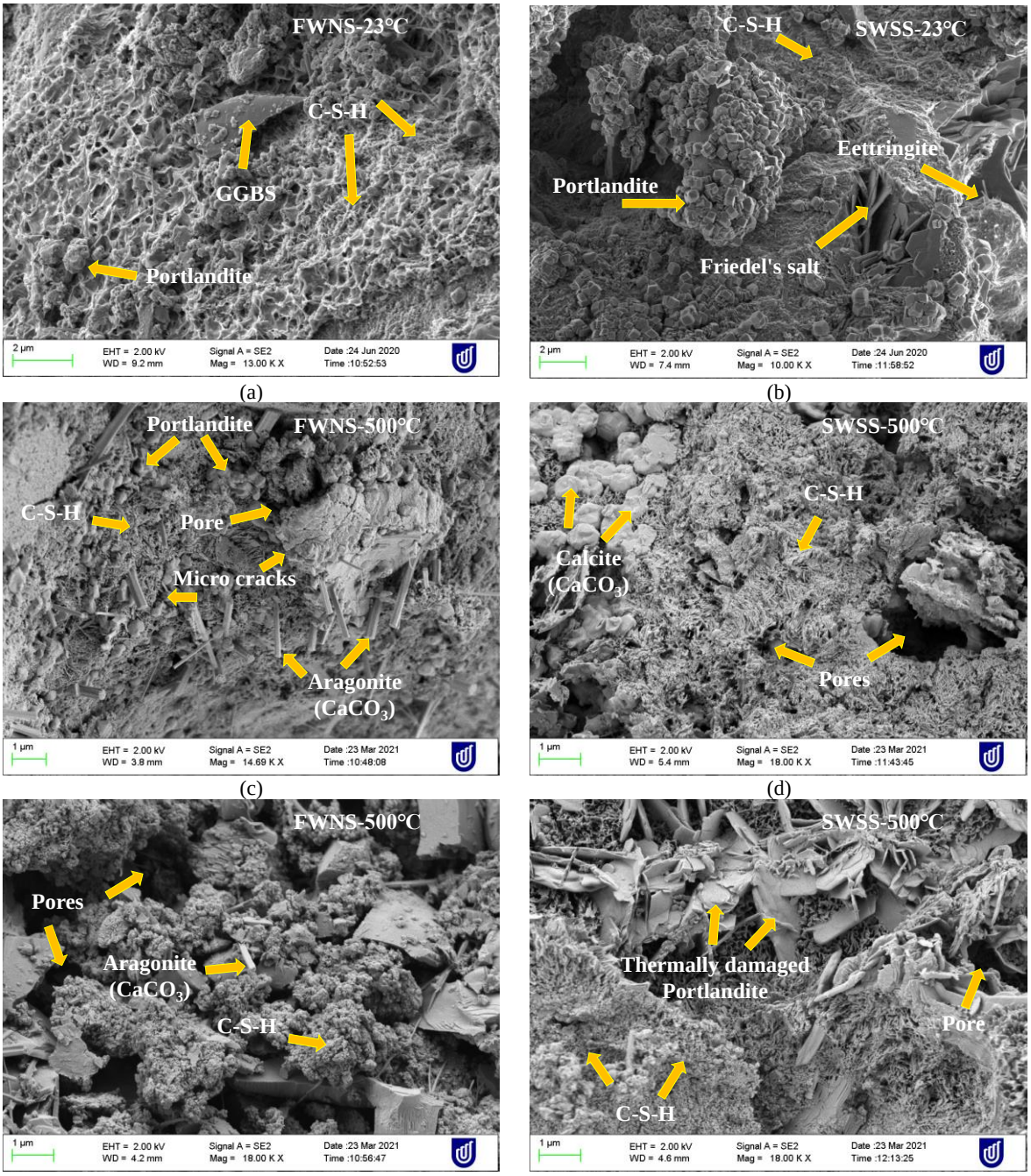
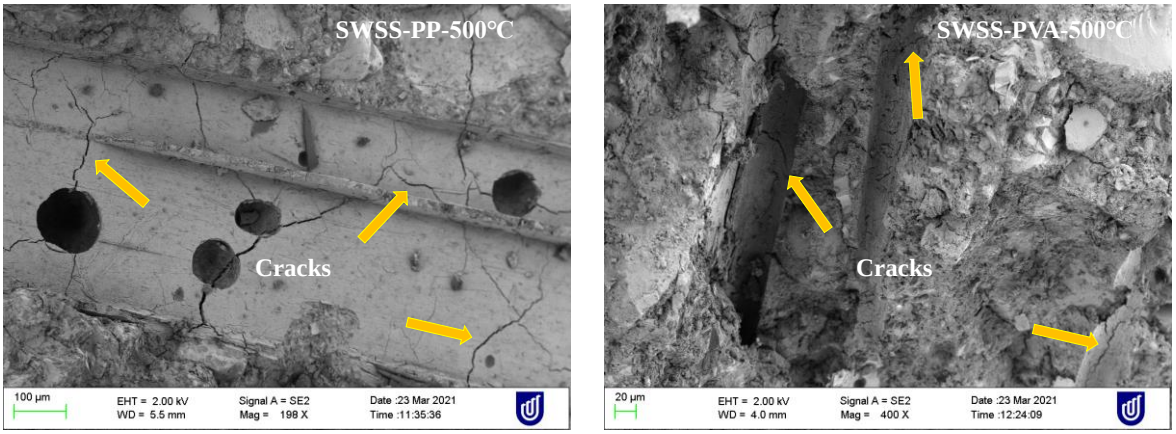


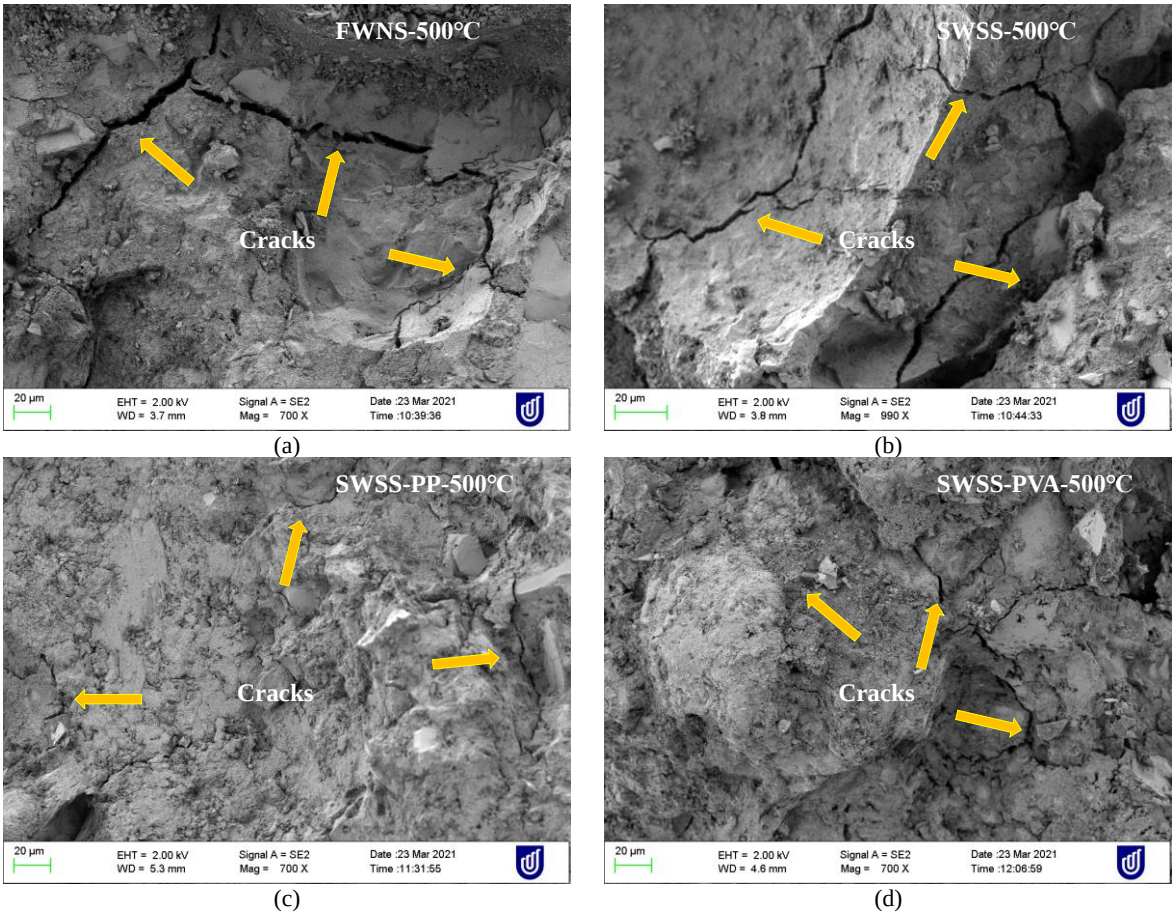
Fig. 14. SEM images of the plain concrete mixes, (a) FWNS at 23 °C, (b) SWSS at 23 °C, (c and e) FWNS after exposure to 500 °C, and (d and f) SWSS after exposure to 500 °C



(a) (b)

Fig. 15. SEM images of (a) PP and (b) PVA fibre beds after melting and burning out of fibre, heating to 500 °C

The cracks' formations in plain and fibre-reinforced specimens after exposure to 500 °C are shown in Fig. 16. Larger and continuous cracks were observed clearly at the surface of both FWNS and SWSS mixes, while the addition of fibre was seen to lead to the formation of only some finer cracks. As discussed before, these finer cracks were due to the additional porosity created by fibre decomposition which provided extra void spaces for concrete expansion.



(a) (b)

(c) (d)

Fig. 16. SEM images of (a) FWNS, (b) SWSS, (c) SWSS-PP, and (d) SWSS-PVA mixes after exposure to 500 °C

3.2.3. Porosity and Water absorption

Water absorption results of all concrete mixes after elevated temperatures are displayed in Table 10 and Fig. 17. Generally, by increasing exposure temperature the concrete porosity increased and more water

absorption values were obtained. At 100 and 300 ℃, SWSS showed lower water absorption than FWNS. While at 500 and 750 ℃ more water absorption was exhibited in SWSS. These observations could be related to the difference in particle sizes and decomposition of SS and NS. At 100 ℃, the effect of PP fibres was not significant. But by using PVA fibres more water absorption was observed compared with plain SWSS mix. At other exposure temperatures, both types of fibre addition led to a decrease in water absorption values. The reasons could be (i) additional voids created by fibres which resulted in a partial release in internal pressure, and consequently, lower and finer cracks formation (Fig. 16), and (ii) filling up the large voids by concrete expansion. As shown in Fig. 17(b), up to 0.3% fibre usage, the more fibre was used, the less water was absorbed. Then it slightly increased with increasing fibre content to 0.5%. Therefore, at elevated temperatures, for both types of PP and PVA fibres, the optimum fibre content to reach the lowest water absorption value was 0.3% fibre volume fraction in this study. Furthermore, to reach lower water absorption, PP fibre was more efficient at lower temperatures, and PVA was more efficient at 500 and 750 ℃.

Table 10. Water absorption results.

Mix ID	Water absorption (%)								
	23 ℃	100 ℃		300 ℃		500 ℃		750 ℃	
FWNS	3.7%	5.0%	(71.5%)	6.9%	(136.48%)	8.0%	(173.29%)	11.9%	(307.15%)
SWSS	2.9%	3.8%	(30%)	6.7%	(127.43%)	8.4%	(186.76%)	12.9%	(342.11%)
SWSS-PP0.1	2.9%	3.8%	(28.84%)	6.0%	(105.61%)	8.4%	(185.56%)	12.2%	(315.55%)
SWSS-PP0.2	3.0%	3.8%	(28.75%)	5.8%	(98.78%)	7.5%	(157.36%)	12.0%	(309.61%)
SWSS-PP0.3	2.9%	3.6%	(24.15%)	5.7%	(95.42%)	7.8%	(167.44%)	11.7%	(300.91%)
SWSS-PP0.5	3.0%	3.7%	(27.63%)	5.8%	(97.28%)	8.0%	(174.9%)	12.3%	(321.4%)
SWSS-PVA0.1	2.7%	3.6%	(24.07%)	6.7%	(127.78%)	7.7%	(161.74%)	12.1%	(312.79%)
SWSS-PVA0.2	3.1%	4.1%	(41.47%)	6.5%	(123.2%)	7.5%	(154.79%)	12.2%	(315.89%)
SWSS-PVA0.3	3.2%	4.2%	(42.54%)	5.5%	(87.58%)	7.2%	(144.43%)	10.3%	(252.61%)
SWSS-PVA0.5	3.4%	4.4%	(51.04%)	6.2%	(110.71%)	7.5%	(157.99%)	9.4%	(222.48%)

Note: The number in the () shows the percentage of water absorption increase over that of the SWSS mix at 23 ℃.

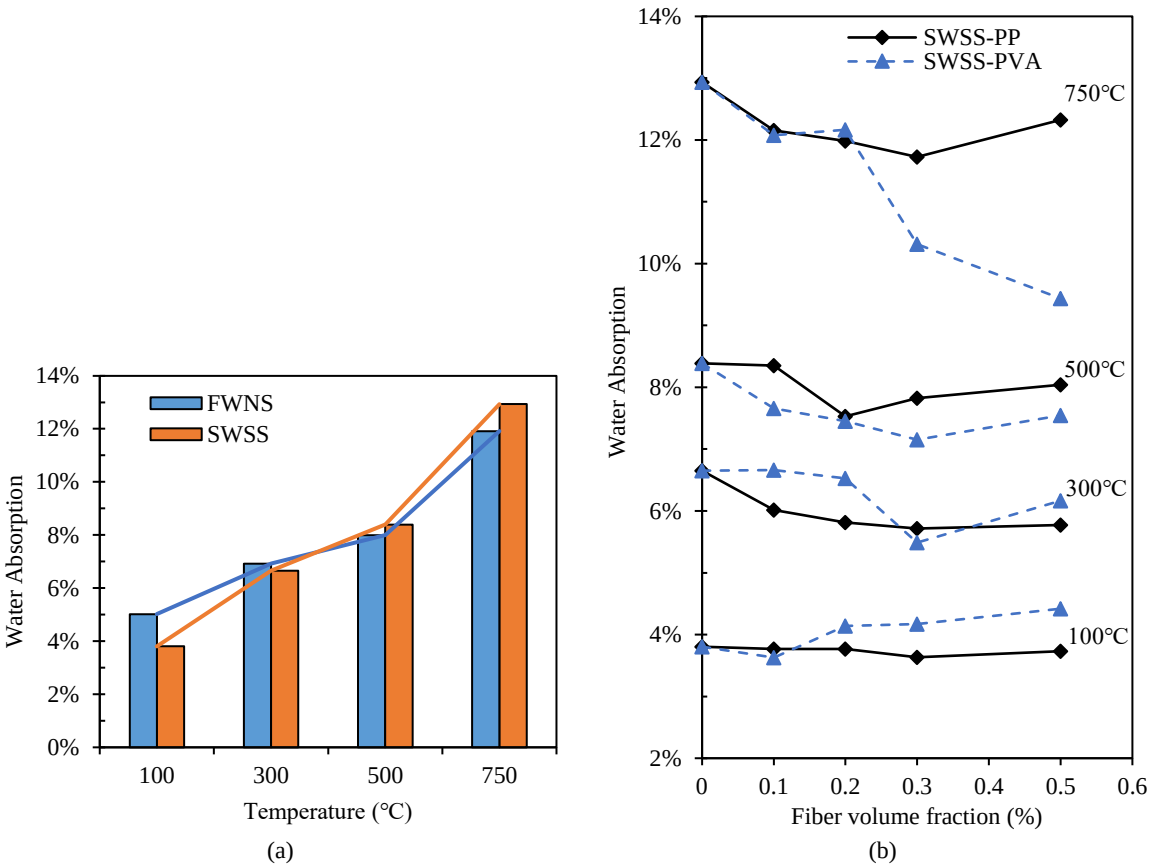
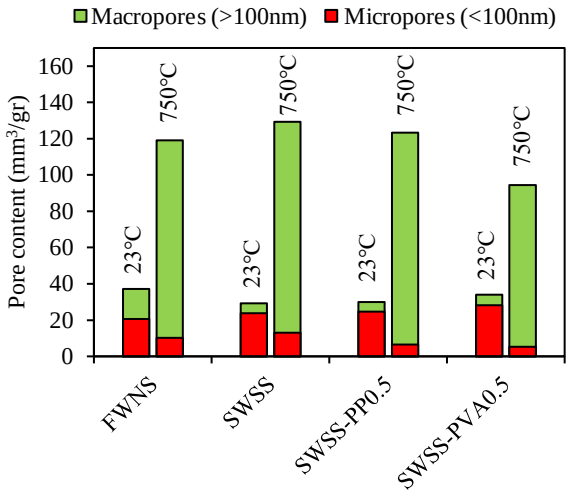


Fig. 17. Water absorption for a) plain and b) fibre-reinforced mixes.

Fig. 18 displays the total porosity as well as the volume of macro- and micro-pores for FWNS, SWSS, SWSS-PP0.5, and SWSS-PVA0.5 mixes after exposure to 23 and 750 ℃. In this figure, the total porosity was measured from the water absorption test. For micro-pores, nitrogen adsorption test using ASAP 2420 system was applied. At room temperature, higher total porosity was observed for FWNS than SWSS, although SWSS had higher micro-pores. Adding fibre to SWSS mix slightly increased micro-pore content while their effect on macro-pores was much less significant. Micro-pore contents of SWSS, SWSS-PP0.5, and SWSS-PVA0.5 mixes at room temperature were 37.75, 24.69, and 28.24 mm^3/gr, respectively, while macro-pore contents were 5.50, 5.29, and 5.74 mm^3/gr, respectively. For all mixes, by increasing temperature from 23 to 750 ℃ a significant increase in total porosity was observed. The average total porosity of the mixes at 750 ℃ was 257% higher than that at room temperature. Interestingly by increasing exposure temperature, while the volume of macro-pores increased, a reduction in micro-pores was obtained. This is attributed to the decomposition of C-S-H and portlandite which opened the pore system of cement paste and increased the total porosity [69]. At 750 ℃ the total porosity of the SWSS, as well as both micro- and macro-pore contents, were slightly higher than FWNS; the effect of PP fibre on total porosity was marginal while PVA fibre addition led to a 27% reduction in the total porosity of SWSS.



Mix ID	Pore content at 23 ℃ (mm^3/gr)			Pore content at 750 ℃ (mm^3/gr)		
	Micropores (<100nm)	Macropores (>100nm)	Total porosity	Micropores (<100nm)	Macropores (>100nm)	Total porosity
FWNS	20.55	16.61	37.16	10.20	108.90	119.11
SWSS	23.75	5.50	29.25	13.11	116.22	129.33
SWSS-PP0.5	24.69	5.29	29.99	6.50	116.77	123.27
SWSS-PVA0.5	28.24	5.74	33.99	5.28	89.06	94.34

Fig. 18. Pore content of the concrete specimens at room and 750 ℃ temperatures.

4. Conclusions

In this study, the properties of a high-strength concrete produced by seawater (SW), dredged sea-sand (DSS), and reinforced with fibres were investigated at the elevated temperatures of 100, 300, 500, and 750°C. The results were compared with those of conventional concrete. Moreover, the effects of polypropylene (PP) and polyvinyl alcohol (PVA) fibres on the properties of seawater sea-sand (SWSS) concrete were examined by incorporation of 0.1% to 0.5% fibre dosages. From the experimental results, it can be concluded that:

1- SWSS mix exhibited lower mass loss compared to that of the FWNS. Effects of fibres on mass loss of SWSS mixes at 100 ℃ was marginal. At higher temperatures, slightly lower mass loss occurred in fibre-reinforced SWSS mixes compared to that of plain concrete. Additional porosity produced by fibre decomposition led to the formation of the finer and less cracks in fibre-reinforced mixes after exposure to elevated temperatures. Compared with PP fibre, more uniform distribution of PVA fibres throughout the concrete mass resulted in a more uniform additional porosity, a higher release of the internal pressure, and superior control on concrete cracking.

2- Despite the exposure temperature, the SWSS concrete mix exhibited a higher residual thermal strain than that of FWNS. Adding PP fibres resulted in an increase in the residual strain of SWSS mix while incorporating PVA fibres reduced the residual strain. By increasing PP and PVA fibre content a further increase and decrease in residual strain occurred, respectively.

3- After exposure to elevated temperatures, the SWSS mix showed slightly lower residual compressive strength, elastic modulus, and tensile strength compared with those of FWNS. Almost similar flexural strength results occurred for both of the mixes.

4- Adding PP fibre to the SWSS mix resulted in a decreased compressive strength after exposure to elevated temperatures. On the contrary, higher compressive strength was achieved for mixes with PVA fibres than plain SWSS. A further increase and decrease in compressive strength were observed by increasing PP and PVA fibre content, respectively. The effect of fibres on the elastic modulus, regardless of the fibre type and content, was marginal.

5- Fibre addition led to an improvement in flexural and tensile strengths of SWSS mixes at all the exposure temperatures. After exposure to 100 ℃, an increasing trend in flexural and tensile strengths was observed when the fibre content increased. The maximum strengths were obtained using the optimum fibre dosage of 0.3%. At higher temperatures, the maximum flexural and tensile strengths were achieved with 0.1% fibre addition, and then the strengths decreased with increasing fibre contents. In this study, PVA fibre exhibited a better contribution in improving concrete strengths compared with PP fibre.

6- For all concrete mixes, an increase in the exposure temperature led to a higher loss in mass, formation of wider cracks with larger numbers, and higher residual strain. Compressive strength, modulus of elasticity, flexural and splitting tensile strength decreased with increasing exposure temperatures. By increasing temperature to 750 ℃, the volume of concrete micro-pores decreased, while total porosity increased.

7- Effects of SW and SS on fracture toughness of the concrete mixes was marginal. For both plain SWSS and FWNS mixes, despite exposure temperature, almost similar pre-crack behaviour, equal peak loads, and the same post-cracking performance with a brittle failure exhibited. The fracture energy of the FWNS and SWSS was almost similar. For both mixes, a wider curve with more ductility was achieved at higher temperatures. The fracture energy of SWSS and FWNS after subjecting to 100, 300, and 500 ℃ was almost equal to that at 23 ℃.

8- At low temperatures, adding PP fibre significantly increase the ductility, post-crack residual strength and fracture energy of the SWSS mix, while PVA fibre showed minor effects. Unlike low temperatures observations, inferior post-crack behaviour and fracture energy of SWSS were obtained by incorporation of PP fibre after subjecting to 300, 500, and 750 ℃. PVA fibre showed no significant effect on the toughness behaviour of SWSS after exposure to these high temperatures.

9- At 100 and 300 ℃, more water was absorbed by FWNS, while at 500 and 750 ℃, SWSS exhibited a higher water absorption value. Generally, adding fibre resulted in a reduced water absorption value of specimens after exposure to elevated temperatures. PP fibre was more efficient at lower temperatures, while PVA was more efficient at 500 and 750 ℃.

10- At 23 ℃, while the total porosity of SWSS was lower than FWNS, higher micro-pores exhibited for SWSS. Adding fibre to SWSS mix slightly increased micro-pore content while its effect on macro-pores was less significant. After subjecting to 750 ℃, while the volume of macro-pores increased, a reduction in micro-pores occurred. Furthermore, the total porosity and the volume of both micro- and macro-pores of the SWSS mix were slightly higher than FWNS.

Overall, this study demonstrated that the incorporation of synthetic fibers, especially PVA fibers, in seawater sea-sand concrete can control concrete cracking and improve its resistance against elevated temperatures. Though this research was the first study in this area, the experimental results revealed that this type of concrete can be used in any type of structure that is susceptible to an incidence of a fire or any other extreme heat source. However, more research examinations on the properties and microstructural behaviour of fibre-reinforced SWSS concrete under elevated temperatures are required before any implementation of this new type of concrete in the construction industry. The new type of fiber-reinforced concrete may provide a better replacement for conventional concrete in building the offshore structure platforms for oil and gas production in terms of fire protection.

Acknowledgements

The authors would like to express their sincere appreciation to the University of South Australia for providing laboratory support and Australian Research Training Program for providing research fund for the first author. The authors also thank Dr. Murray Townsend and Mr. Mojtaba Karbasi from Department for Environment and Water (DEW) and Mr. Spiros Dimas from Department of Infrastructure and Transport (DIT) of the Government of South Australia for their kind assistance in dredged sea-sand supply. The donation of OPC and GGBS from Adelaide Brighton Cement Ltd, and Independent Cement and Lime Pty Ltd, respectively, is greatly appreciated.

References

[1] B. Bajželj, J.M. Allwood, J.M. Cullen, Designing Climate Change Mitigation Plans That Add Up, Environmental Science & Technology 47(14) (2013) 8062-8069.
[2] UNWWD, The United Nations world water development report 2018: nature-based solutions for water, UNESCO, Paris, 2018.
[3] P. Peduzzi, Sand, rarer than one thinks, Environmental Development 11 (2014) 208-218.
[4] S.A. Miller, A. Horvath, P.J.M. Monteiro, Impacts of booming concrete production on water resources worldwide, Nature Sustainability 1(1) (2018) 69-76.
[5] A. Gholampour, T. Ozbakkaloglu, T.D. Ngo, Development of a waste-based eco-friendly structural mortar without Portland cement and natural sand, Structural Concrete 22(S1) (2021) E488-E500.
[6] Y. Li, C. Qiao, W. Ni, Green concrete with ground granulated blast-furnace slag activated by desulfurization gypsum and electric arc furnace reducing slag, Journal of Cleaner Production 269 (2020) 122212.
[7] N. Gupta, R. Siddique, R. Belarbi, Sustainable and Greener Self-Compacting Concrete incorporating Industrial By-Products: A Review, Journal of Cleaner Production 284 (2021) 124803.
[8] M.I. Khan, 14 - Nanosilica/silica fume, Waste and Supplementary Cementitious Materials in Concrete, Woodhead Publishing2018, pp. 461-491.
[9] M.C. Collivignarelli, A. Abbà, M. Carnevale Miino, G. Cillari, P. Ricciardi, A review on alternative binders, admixtures and water for the production of sustainable concrete, Journal of Cleaner Production 295 (2021) 126408.
[10] K.M. Rahla, R. Mateus, L. Bragança, Comparative sustainability assessment of binary blended concretes using Supplementary Cementitious Materials (SCMs) and Ordinary Portland Cement (OPC), Journal of Cleaner Production 220 (2019) 445-459.
[11] T. Dhondy, A. Remennikov, M.N. Shiekh, Benefits of using sea sand and seawater in concrete: a comprehensive review, Australian Journal of Structural Engineering 20(4) (2019) 280-289.
[12] J. Xiao, C. Qiang, A. Nanni, K. Zhang, Use of sea-sand and seawater in concrete construction: Current status and future opportunities, Construction and Building Materials 155 (2017) 1101-1111.

[13] D. Vafaei, X. Ma, R. Hassanli, Y. Zhuge, Effects of Seawater and Sea-Sand on Concrete Properties: A Review Paper, EASEC16, Springer Singapore, Singapore, 2021, pp. 2037-2049.
[14] D. Vafaei, R. Hassanli, X. Ma, J. Duan, Y. Zhuge, Sorptivity and mechanical properties of fiber-reinforced concrete made with seawater and dredged sea-sand, Construction and Building Materials (2020) 121436.
[15] D. Vafaei, X. Ma, R. Hassanli, J. Duan, Y. Zhuge, Microstructural behaviour and shrinkage properties of high-strength fiber-reinforced seawater sea-sand concrete, Construction and Building Materials 320 (2022) 126222.
[16] D. Vafaei, R. Hassanli, X. Ma, J. Duan, Y. Zhuge, Fracture Toughness and Impact Resistance of Fiber-Reinforced Seawater Sea-Sand Concrete, Journal of Materials in Civil Engineering (ASCE) (2021).
[17] F. Guo, S. Al-Saadi, R.K. Singh Raman, X.L. Zhao, Durability of fiber reinforced polymer (FRP) in simulated seawater sea sand concrete (SWSSC) environment, Corrosion Science 141 (2018) 1-13.
[18] A. Younis, U. Ebead, S. Judd, Life cycle cost analysis of structural concrete using seawater, recycled concrete aggregate, and GFRP reinforcement, Construction and Building Materials 175 (2018) 152-160.
[19] M. Khatibmasjedi, S. Ramanathan, P. Suraneni, A. Nanni, Durability of Commercially Available GFRP Reinforcement in Seawater-Mixed Concrete under Accelerated Aging Conditions, Journal of Composites for Construction 24(4) (2020) 04020026.
[20] Z. Dong, G. Wu, X.-L. Zhao, H. Zhu, J.-L. Lian, Durability test on the flexural performance of seawater sea-sand concrete beams completely reinforced with FRP bars, Construction and Building Materials 192 (2018) 671-682.
[21] F. Yan, Z. Lin, Bond durability assessment and long-term degradation prediction for GFRP bars to fiber-reinforced concrete under saline solutions, Composite Structures 161 (2017) 393-406.
[22] M. Reid, The Piper Alpha Disaster: A Personal Perspective with Transferrable Lessons on the Long-Term Moral Impact of Safety Failures, ACS Chemical Health & Safety 27(2) (2020) 88-95.
[23] Deep water : the Gulf oil disaster and the future of offshore drilling : report to the President, United States. National Commission on the, B. P. Deepwater Horizon Oil Spill Offshore, Drilling (2011).
[24] J.K. Seo, S.E. Lee, J.S. Park, A method for determining fire accidental loads and its application to thermal response analysis for optimal design of offshore thin-walled structures, Fire Safety Journal 92 (2017) 107-121.
[25] B. Georgali, P.E. Tsakiridis, Microstructure of fire-damaged concrete. A case study, Cement and Concrete Composites 27(2) (2005) 255-259.
[26] K. Scrivener, R. Snellings, B. Lothenbach, A Practical Guide to Microstructural Analysis of Cementitious Materials, Boca Raton: CRC Press2016.
[27] W. Sha, - Differential scanning calorimetry study of the hydration products in portland cement pastes with metakaolin replacement, Advances in Building Technology, Elsevier, Oxford, 2002, pp. 881-888.
[28] P. Kalifa, G. Chéné, C. Gallé, High-temperature behaviour of HPC with polypropylene fibres: From spalling to microstructure, Cement and Concrete Research 31(10) (2001) 1487-1499.
[29] F. Aslani, B. Samali, High Strength Polypropylene Fibre Reinforcement Concrete at High Temperature, Fire Technology 50(5) (2014) 1229-1247.
[30] N.N. Albert, Temperature Distribution and Mechanical Properties of High-Strength Silica Fume Concrete at Temperatures up to 200 °C, ACI Materials Journal 100(4).
[31] J. Xiao, H. Falkner, On residual strength of high-performance concrete with and without polypropylene fibres at elevated temperatures, Fire Safety Journal 41(2) (2006) 115-121.
[32] M. Zeiml, D. Leithner, R. Lackner, H.A. Mang, How do polypropylene fibers improve the spalling behavior of in-situ concrete?, Cement and Concrete Research 36(5) (2006) 929-942.
[33] A.A. Deshpande, D. Kumar, R. Ranade, Influence of high temperatures on the residual mechanical properties of a hybrid fiber-reinforced strain-hardening cementitious composite, Construction and Building Materials 208 (2019) 283-295.
[34] A. Çavdar, A study on the effects of high temperature on mechanical properties of fiber reinforced cementitious composites, Composites Part B: Engineering 43(5) (2012) 2452-2463.
[35] H. Mohammadhosseini, J.M. Yatim, Microstructure and residual properties of green concrete composites incorporating waste carpet fibers and palm oil fuel ash at elevated temperatures, Journal of Cleaner Production 144 (2017) 8-21.
[36] Y.-L. Li, X.-L. Zhao, R.K. Singh Raman, S. Al-Saadi, Thermal and mechanical properties of alkali-activated slag paste, mortar and concrete utilising seawater and sea sand, Construction and Building Materials 159 (2018) 704-724.
[37] X. Geng, M.C. Boufadel, N.L. Jackson, Evidence of salt accumulation in beach intertidal zone due to evaporation, Sci Rep 6 (2016) 31486-31486.
[38] AS 3600, Concrete Structures, Standards Australia, Sydney, N.S.W, 2018.
[39] AS 4997, Guidelines for the design of maritime structures, Standards Australia, Sydney, N.S.W, 2005.

[40] H.R. Pakravan, T. Ozbakkaloglu, Synthetic fibers for cementitious composites: A critical and in-depth review of recent advances, Construction and Building Materials 207 (2019) 491-518.
[41] P. Zhang, Y. Yang, J. Wang, M. Jiao, Y. Ling, Fracture Models and Effect of Fibers on Fracture Properties of Cementitious Composites-A Review, Materials (Basel, Switzerland) 13(23) (2020).
[42] AS 1012.2, Methods of testing concrete - Preparation of concrete mixes in the laboratory, Standards Australia, Sydney, N.S.W, 2014.
[43] AS 1012.17, Methods of testing concrete - Methods for the determination of the static chord modulus of elasticity and Poisson's ratio of concrete specimens, Standards Australia, Sydney, N.S.W, 1976.
[44] AS 1012.11, Methods of testing concrete - Method for the determination of the flexural strength of concrete specimens, Standards Australia, Sydney, N.S.W, 1985.
[45] AS 1012.10, Methods of testing concrete - Determination of indirect tensile strength of concrete cylinders ('Brazil' or splitting test), Standards Australia, Sydney, N.S.W, 2000.
[46] JCI-S-002-2003, Method of test for load-displacement curve of fiber reinforced concrete by use of notched beam, Japan Concrete Institute Standard2003.
[47] AS 1012.21, Methods of testing concrete - Determination of water absorption and apparent volume of permeable voids in hardened concrete, Standards Australia, Sydney, N.S.W, 1999.
[48] G. De Schutter, K. Audenaert, Evaluation of water absorption of concrete as a measure for resistance against carbonation and chloride migration, Materials and Structures 37(9) (2004) 591.
[49] F. Gong, D. Zhang, E. Sicat, T. Ueda, Empirical Estimation of Pore Size Distribution in Cement, Mortar, and Concrete, Journal of Materials in Civil Engineering 26(7) (2014) 04014023.
[50] L.P. Esteves, On the hydration of water-entrained cement–silica systems: Combined SEM, XRD and thermal analysis in cement pastes, Thermochimica Acta 518(1) (2011) 27-35.
[51] P.D. P. Kumar Mehta, P.D. Paulo J. M. Monteiro, Concrete: Microstructure, Properties, and Materials, Fourth Edition, 4th ed. ed., McGraw-Hill Education, New York, 2014.
[52] P. Thongsanitgarn, W. Wongkeo, A. Chaipanich, Hydration and Compressive Strength of Blended Cement Containing Fly Ash and Limestone as Cement Replacement, Journal of Materials in Civil Engineering 26(12) (2014) 04014088.
[53] M.A. Tantawy, Effect of high temperatures on the microstructure of cement paste, Journal of Materials Science and Chemical Engineering 5 (2017) 33-48.
[54] R. Vedalakshmi, A. Sundara Raj, S. Srinivasan, K. Ganesh Babu, Quantification of hydrated cement products of blended cements in low and medium strength concrete using TG and DTA technique, Thermochimica Acta 407(1) (2003) 49-60.
[55] L. Black, Low clinker cement as a sustainable construction material, Sustainability of Construction Materials, Woodhead Publishing2016, pp. 415-457.
[56] P. Li, W. Li, T. Yu, F. Qu, V.W.Y. Tam, Investigation on early-age hydration, mechanical properties and microstructure of seawater sea sand cement mortar, Construction and Building Materials 249 (2020) 118776.
[57] G. Gan, The Role of Magnesium in Concrete Deterioration, Iowa State University1996.
[58] Z. Shi, M.R. Geiker, B. Lothenbach, K. De Weerdt, S.F. Garzón, K. Enemark-Rasmussen, J. Skibsted, Friedel's salt profiles from thermogravimetric analysis and thermodynamic modelling of Portland cement-based mortars exposed to sodium chloride solution, Cement and Concrete Composites 78 (2017) 73-83.
[59] L.D. Mitchell, J.C. Margeson, Theeffects of solvents on C–S–H as determined by thermal analysis, Journal of Thermal Analysis and Calorimetry 86(3) (2006) 591-594.
[60] H. AzariJafari, M.J. Taheri Amiri, A. Ashrafian, H. Rasekh, M.J. Barforooshi, J. Berenjian, Ternary blended cement: An eco-friendly alternative to improve resistivity of high-performance self-consolidating concrete against elevated temperature, Journal of Cleaner Production 223 (2019) 575-586.
[61] A.M. Rashad, An investigation of high-volume fly ash concrete blended with slag subjected to elevated temperatures, Journal of Cleaner Production 93 (2015) 47-55.
[62] S.L. Suhaendi, T. Horiguchi, Effect of short fibers on residual permeability and mechanical properties of hybrid fibre reinforced high strength concrete after heat exposition, Cement and Concrete Research 36(9) (2006) 1672-1678.
[63] R. Gül, E. Okuyucu, İ. Türkmen, A.C. Aydin, Thermo-mechanical properties of fiber reinforced raw perlite concrete, Materials Letters 61(29) (2007) 5145-5149.
[64] D. Ríos José, H. Cifuentes, C. Leiva, C. García, D. Alba María, Behavior of High-Strength Polypropylene Fiber-Reinforced Self-Compacting Concrete Exposed to High Temperatures, Journal of Materials in Civil Engineering 30(11) (2018) 04018271.
[65] M. Tufail, K. Shahzada, B. Gencturk, J. Wei, Effect of Elevated Temperature on Mechanical Properties of Limestone, Quartzite and Granite Concrete, International Journal of Concrete Structures and Materials 11(1) (2017) 17-28.

[66] W. Khaliq, V. Kodur, Thermal and mechanical properties of fiber reinforced high performance self-consolidating concrete at elevated temperatures, Cement and Concrete Research 41(11) (2011) 1112-1122.
[67] M.S. Magalhães, R.D. Toledo Filho, E.M.R. Fairbairn, Durability under thermal loads of polyvinyl alcohol fibers Matéria (Rio de Janeiro) 18 (2013) 1587-1595.
[68] J.D. Menczel, 4-Thermogravimetric analysis of fibers, Thermal Analysis of Textiles and Fibers, Woodhead Publishing2020, pp. 71-79.
[69] M. Saad, S.A. Abo-El-Enein, G.B. Hanna, M.F. Kotkata, Effect of temperature on physical and mechanical properties of concrete containing silica fume, Cement and Concrete Research 26(5) (1996) 669-675.